Nano-Micro Letters

e-ISSN 2150-5551
CN 31-2103/TB

REVIEW

https://doi.org/10.1007/s40820-025-01672-w

Cite as
Nano-Micro Lett.
(2025) 17:175

Received: 22 September 2024
Accepted: 17 January 2025

V–Ti-Based Solid Solution Alloys for Solid-State Hydrogen Storage

Shaoyang Shen[1], Yongan Li[1], Liuzhang Ouyang[1] ✉, Lan Zhang[2,3], Min Zhu[1,2], Zongwen Liu[4,5] ✉

HIGHLIGHTS

- Hydrogen storage performance of V-Ti-based solid solution alloys is related to the elementary composition, phase structure, and homogeneity.
- Micro-strain accumulation is responsible for capacity degradation.
- Low-cost and high-performance V-Ti-based solid solution alloys with high reversible hydrogen storage capacity, good cyclic durability, and excellent activation performance should be developed.

ABSTRACT This review details the advancement in the development of V–Ti-based hydrogen storage materials for using in metal hydride (MH) tanks to supply hydrogen to fuel cells at relatively ambient temperatures and pressures. V–Ti-based solid solution alloys are excellent hydrogen storage materials among many metal hydrides due to their high reversible hydrogen storage capacity which is over 2 wt% at ambient temperature. The preparation methods, structure characteristics, improvement methods of hydrogen storage performance, and attenuation mechanism are systematically summarized and discussed. The relationships between hydrogen storage properties and alloy compositions as well as phase structures are discussed emphatically. For large-scale applications on MH tanks, it is necessary to develop low-cost and high-performance V–Ti-based solid solution alloys with high reversible hydrogen storage capacity, good cyclic durability, and excellent activation performance.

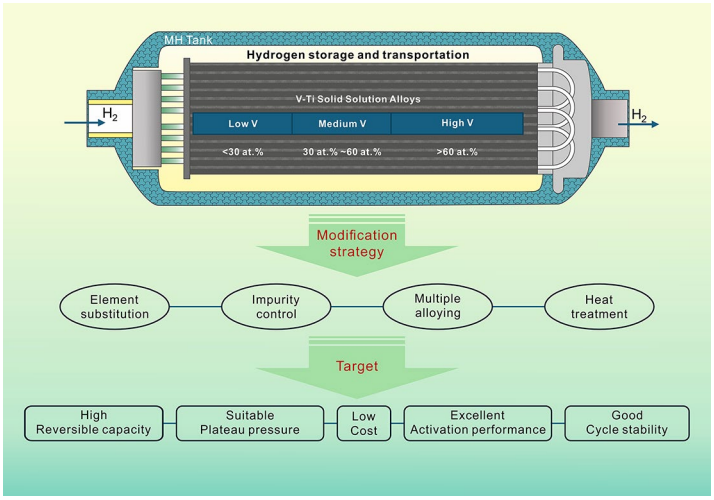

KEYWORDS Hydrogen storage; V–Ti-based solid solution alloys; Metal hydride tank; Hydrogen storage properties; Cyclic stability

Shaoyang Shen and Yongan Li contributed equally to this work.

✉ Liuzhang Ouyang, meouyang@scut.edu.cn; Zongwen Liu, zongwen.liu@sydney.edu.au
[1] School of Materials Science and Engineering and Key Laboratory of Advanced Energy Storage Materials of Guangdong Province, South China University of Technology, Guangzhou 510641, People's Republic of China
[2] Energy Research Institute at NTU (ERI@N), Nanyang Technological University, 1 CleanTech Loop, Singapore 637141, Singapore
[3] China-Singapore International Joint Research Institute (CSIJRI), Guangzhou 510530, People's Republic of China
[4] Institute of Fundamental and Frontier Sciences, University of Electronic Science and Technology of China, Chengdu 610054, People's Republic of China
[5] School of Chemical and Biomolecuar Engineering, The University of Sydney, Sydney, NSW 2006, Australia

Published online: 04 March 2025

1 Introduction

Solid-state hydrogen storage technology has received widespread attention because of the application of hydrogen energy in full swing and the requirement of high volumetric and gravimetric density candidates [1–3]. For on-board hydrogen storage, the vehicle-mounted hydrogen storage device is a reservoir that supplies hydrogen to fuel cells, which also requires a suitable hydrogen absorption/desorption rate at ambient temperature [4], as shown in Fig. 1. Consequently, acceptable economic cost, long cycle life, and safety for complex working conditions are more necessary for on-board hydrogen storage devices. In view of these, solid-state hydrogen storage technology provides an option to store hydrogen under non-extreme conditions (e.g., avoid 70 MPa or − 253 °C) [5].

Traditional hydrogen storage alloys, such as AB_5-type, AB-type, and AB_2-type alloys, typically have hydrogen capacities of less than 2.0 wt% [6, 7]. Despite the magnesium-based alloys having a higher hydrogen capacity (7.6 wt%), their high dehydrogenation temperature limits their application in on-board hydrogen storage devices [8–12]. Of course, by adding catalysts or applying nanoscale techniques, the dehydrogenation temperature can be effectively reduced while maintaining a hydrogen storage capacity above 6 wt% [13–15]. However, the actual dehydrogenation temperature is still difficult to match with the fuel cell module [16–18]. Metal borohydrides face a similar dilemma, and there is also the cost to consider [19]. Although the cost can be reduced by regenerating metal borohydrides from hydrolyzed products, further research is needed in terms of high dehydrogenation temperature, slow dehydrogenation kinetics and poor reversibility [20–22]. Reassuringly, V–Ti-based solid solution alloys exhibit a reversible hydrogen storage capacity of over 2.0 wt% at temperatures below 100 °C and are expected to be used on solid-state hydrogen storage devices [23, 24].

V–Ti-based solid solution alloys have been widely used and replaced metal V in many application areas because of their high hydrogen storage capacity, suitable hydrogen equilibrium pressure, and good anti-pulverization performance, such as solid-state hydrogen storage [25–27], Ni-MH battery [28–31], hydrogen separation [32–34], and hydrogen isotope effect [35]. However, since both V and Ti are hydrogen-stable metals, the resulting V–Ti alloy is also hydrogen-stable. For practical applications, it also encounters issues such as low effective hydrogen storage capacity, an uneven plateau area, and limited cyclic durability [23]. Therefore, multiple metallic elements are often simultaneously added to the alloy, forming a wide varieties of V–Ti-based hydrogen storage alloys with diverse properties.

This review summarizes the research progress of V–Ti-based solid solution alloys in recent years. The preparation methods, compositions, crystal structures, modification methods, and hydrogen storage properties of V–Ti-based solid solution alloys are fully discussed in this article.

2 Preparation and Structural Characteristics of V–Ti-Based Solid Solution Alloys

The metal V and Ti can be mutually soluble in any proportion, forming an infinite solid solution with a nearly 4 wt% hydrogen storage capacity. Since Akiba et al. [36] proposed the concept of "Laves phase-related BCC solid solution," researchers have paid more attention to the V–Ti-based solid solution alloys. Generally, the V–Ti-based solid solution alloys change from the BCC phase (α phase) to the BCT phase (β phase) in the process of hydrogenation, and the relatively stable monohydride is formed at this stage. After further hydrogen absorption, the BCT phase converts to the FCC phase (γ phase), forming the dihydride. The dehydrogenation pathway of V–Ti-based solid solution alloys can be simply described as $FCC(\gamma) \rightarrow BCT(\beta) \rightarrow BCC(\alpha)$. Both hydrides have a wide range of non-stoichiometric ratios [37]. Therefore, although V–Ti-based solid solution alloys have a high theoretical hydrogen storage capacity of nearly 4 wt%, the actual effective hydrogen storage capacity is only about 2.6 wt% [24]. In fact, only the hydrogen storage capacity involved in phase transformation between the FCC phase and BCT phase is reversible, and the stable BCT phase generally cannot be dehydrogenated at near room temperature. And neutron diffraction results also show that the crystal structure of $Ti_{38}V_{30}Cr_{14}Mn_{18}$ alloy during the hydrogenation process transforms from the initial BCC structure to the BCT structure and then converts to FCC structure, in which the deuterium atoms occupy the octahedral sites of the BCC phase and tetrahedral sites of the BCT and FCC phases [38]. Therefore, the hydrogen absorption and desorption processes of V–Ti-based solid solution alloys can be summarized in Fig. 2 [12].

https://doi.org/10.1007/s40820-025-01672-w

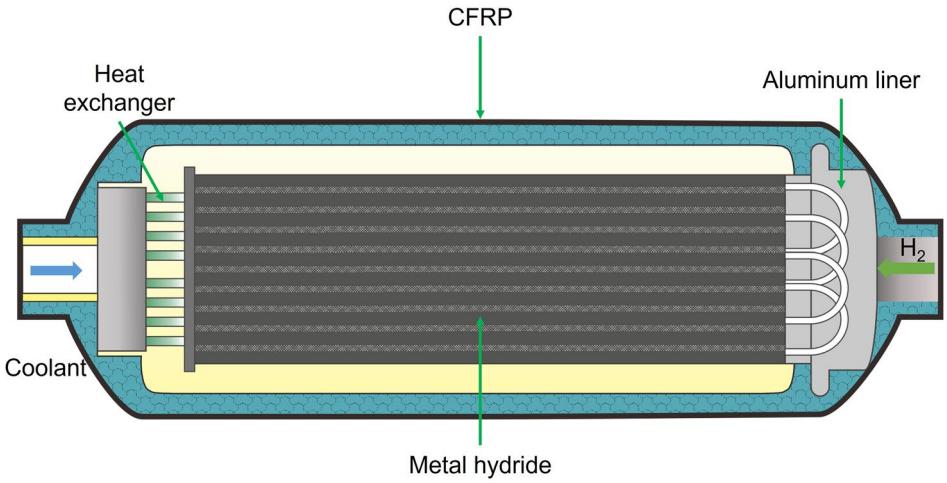

Fig. 1 A schematic view of the MH tank

The preparation of alloys is related to the homogeneity of composition and phase, which is ultimately reflected in the hydrogen storage properties. For V–Ti-based solid solution alloys, in addition to ensuring the uniformity of the alloy, the content of impurities should also be strictly controlled, especially the oxygen content. Further, many of the elements involved in the V–Ti-based solid solution alloys, such as Ti, V, Cr, and Mn, are relatively active elements, which are easy to combine with oxygen to form metal oxides. Therefore, it is of practically significant to develop a suitable preparation process for the fabrication of high-quality and high-performance V–Ti-based solid solution alloys. Several methods, such as arc melting [39–44], vacuum magnetic levitation induction melting [45–48], powder sintering [49, 50], aluminothermy process [51, 52], ball milling [26, 53–59], suction casting [60, 61], floating zone melting [24, 62], rapid solidification [63] and laser engineered net shaping [64], have been used to prepare V–Ti-based solid solution alloys. In addition, heat treatment is also often used in combination with the above preparation methods, which will be detailed below.

Arc melting is the most common method for preparing V–Ti-based solid solution alloys, which is always in conjunction with a water-cooled copper crucible under an argon atmosphere [65]. Aoki et al. [66] prepared $Ti_{12}Cr_{23}V_{65}$ and $Ti_{12}Cr_{23}V_{64}Fe_1$ alloys with single-phase BCC phase by arc melting and the BCC phase of the alloys converted to γ phase with an FCC crystal structure and β phase with a BCT crystal structure during de/hydrogenation, respectively. Yoo et al. [67] obtained $Ti_{0.32}Cr_{0.33}V_{0.25}Mn_{0.1}$ alloy by arc melting under Ar atmosphere with a BCC phase, while the Laves phase appeared with an Mn concentration of 10 at%. Suction casting is beneficial to avoid the formation of the $TiCr_2$ phase, so it is easier to obtain single-phase BCC Ti–Cr–V alloys. For example, the as-cast $(Ti_{0.46}Cr_{0.54})_{95}V_5$ alloy after arc melting consists of $TiCr_2$ phase and BCC phase, while the alloy prepared by suction casting is a single BCC phase [60]. Compared with the as-cast alloy, grain sizes of the rapid solidification alloys were apparently refined and the phase abundance of the BCC phase for $Ti_{0.9}V_{0.1}$ alloy also increased [63].

Powder sintering is considered a suitable option that can be used for the manufacture of V–Ti-based solid solution alloys. Mao et al. [50] synthesized low-cost $(FeV_{80})_{48}Ti_{26}Cr_{26}$ alloy using hydride powder sintering method and the sintered $(FeV_{80})_{48}Ti_{26}Cr_{26}$ alloy could achieve the hydrogen storage properties comparable to the melted sample with Ti compensation. It is worth noting that a cheaper FeV_{80} alloy was used as the raw material and a reversible dehydrogenation capacity of 2.0 wt% was obtained at room temperature.

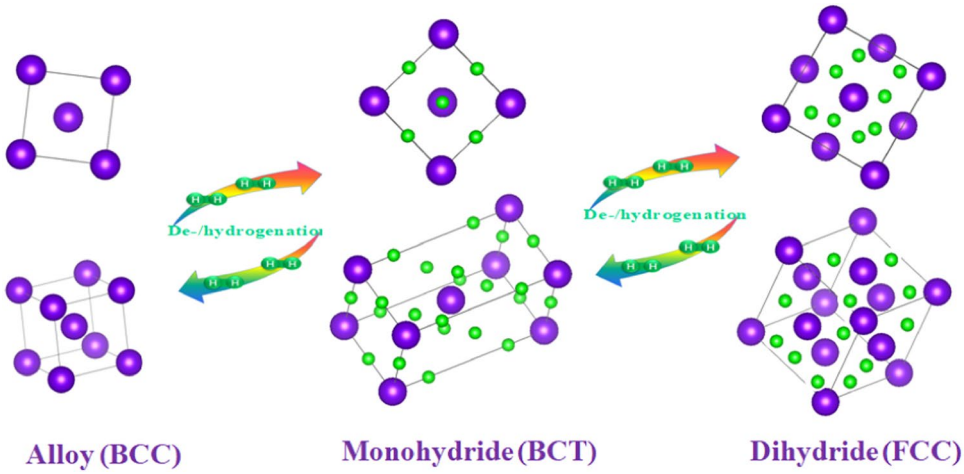

Fig. 2 Schematic of the alloy crystal structure transformation upon de-/hydrogenation [12]. Copyright 2021 Elsevier

Ball milling has also been attempted to prepare V–Ti-based solid solution alloys. Cauceglia et al. [59] prepared the Ti–V–Ni alloy by ball milling, but unfortunately, the reversible hydrogen storage capacity of the alloy was only 1 wt%. Wang et al. [55] reported that the maximum hydrogen storage capacity of the $Ti_{0.37}V_{0.38}Mn_{0.25}$ alloy prepared by mechanical alloying was 1.76 wt%, which was far lower than the capacity of the samples prepared by arc melting (3.62 wt%). The reason is that the samples prepared by arc melting have better crystal structures or crystallinity, which can provide more sites for the absorption of hydrogen atoms. In another study, the hydrogen storage capacity of the alloy decreased with the increase of ball milling time [58]. Therefore, ball milling changes the microstructure of the alloys and reduces grain size while increasing lattice strain and grain boundaries, and can also cause surface contamination [58]. The modification of the alloy prepared by arc melting using ball milling technology can significantly improve the kinetic properties of the alloy samples. The TiZrFeMnCrV alloy prepared by this method has ultra-fast hydrogen absorption kinetics, which can absorb 1.80 wt% hydrogen at a mild condition of 303 K, and the capacity is stable at about 1.76 wt% after 50 cycles, and the material is considered suitable for hydrogen storage in low-power fuel cells [68]. Zadorozhnyy et al. [69] compared the properties of single-phase BCC structured alloys prepared by arc melting (AM), electron beam melting with pendant drop melt extraction (EBM-PDME) as well as mechanical alloying (MA), and concluded that the alloys prepared by the AM and EBM-PDME methods had a hydrogen absorption of 1.6 wt% when fully transformed from the BCC phase to the FCC phase, in contrast to the MA alloy, which underwent partial amorphization and had a hydrogen storage capacity of less than 0.9 wt%. The authors attributed this discrepancy to the different equilibrium states of the alloys resulting from the different preparation processes. The high-temperature synthesis methods (AM and EBM-PDME) allow the metal atoms to occupy stable positions during the transition from the liquid phase to the solid solution, whereas mechanical alloying leads to the formation of highly disordered imperfect crystal structures that make them more susceptible to amorphization.

Like most high melting point alloys, V–Ti-based solid solution alloys can also be prepared by aluminothermic reduction, and the reaction is shown in Eq. (1). The high heat generated during the reaction melts the raw materials, and the product is separated from the Al_2O_3 slag after cooling. Recently, a V_{82}–Ti_{41}–Cr_{73}–$Al_{0.08}$ alloy was prepared by the aluminothermic method followed by vacuum arc melting [51]. This method is simple and inexpensive, but residual aluminum and other impurities will also affect the hydrogen storage properties of the alloy.

$$M_xO_y + Al \rightarrow M + Al_2O_3 \quad (1)$$

The homogeneity of composition and phase significantly impacts the hydrogen storage performance of the alloy. Even after heat treatment, the fluctuation in vanadium concentration between regions with higher and lower vanadium

 https://doi.org/10.1007/s40820-025-01672-w

content typically reaches up to 5%. Itoh and Arashima et al. [24, 62], prepared more homogeneous Ti–Cr–V alloys by floating zone melting and obtained higher reversible hydrogen storage capacity than that of the heat-treated alloys.

In general, researchers have been relentlessly striving to prepare alloys with uniform composition, controllable phase structure, and relatively low cost.

3 Hydrogen Storage Properties of V–Ti-Based Solid Solution Alloys

The V–Ti-based solid solution alloys, as the main materials of the metal hydride tank to supply hydrogen to the fuel cells, need to have the following properties: (1) high reversible volumetric and gravimetric hydrogen capacity at low temperature; (2) suitable plateau pressure; (3) smaller slope factor; (4) good cyclic durability; (5) acceptable economic cost [70, 71]. In general, the hydrogen storage properties of V–Ti-based solid solution alloys are inseparable from their compositions and phase structures and have been extensively studied over the past few decades. Table 1 exhibits the reversible dehydrogenation capacities of some V–Ti-based hydrogen storage alloys at specific temperatures and the corresponding desorption plateau pressures. Based on information from some references, the roles of various elements in the V–Ti-based solid solution alloys are summarized and shown in Table 2.

3.1 Classification of V–Ti-Based Solid Solution Alloys

According to the V content in the alloys, V–Ti solid solution alloys can be divided into high V (> 60 at% V), medium V (30–60 at% V), and low-V (< 30 at%) alloys. For low-V alloys, they are mostly composed of BCC, C14, or C15 phases. For medium and high V alloys, the BCC phase becomes the main phase with increasing V content. Of course, very few CeO_2 and Ti–rich phases appear occasionally, depending on the composition and melting method. In general, low-V alloys tend to have low hydrogen storage capacity due to the presence of more C14 or C15 phases, but on the other hand, such alloys tend to have better activation performance. Besides higher hydrogen storage capacity, alloys with higher V content have better cycle stability due to the smaller bulk elastic modulus. From the initial binary V–Ti alloys to ternary, quaternary, and even quintuple alloys, a great deal of effort has been carried out to alter the hydrogen storage properties of these alloys.

3.2 Composition Modification

Elemental substitution is a commonly used method to prepare V–Ti-based solid solution alloys with varied properties. These added elements can be broadly categorized into two types, hydrogen-stable metals and hydrogen-liable metals. It has been found that these substitutions not only reduce costs but also alter the hydrogen storage properties.

3.2.1 Hydrogen Stable Metal Substitution

The V–Ti-based solid solution alloys with high V content tend to have higher reversible hydrogen storage capacity such as 75V–Ti–15Cr–1Al–1Fe and 75 at%V-5 at%Ti–Cr [39, 70, 83]. Tsukahara et al. [83] obtained a 60 at% V-15 at% Ti-25 at% Cr alloy with a reversible hydrogen storage capacity of up to 2.62 wt% by adjusting the element content in the V–Ti–Cr alloy, demonstrating the potential of this alloy as a hydrogen carrier to supply hydrogen to fuel cells. It is generally believed that high V content can effectively improve the cyclic durability of V–Ti hydrogen storage alloys [24, 108]. Itoh et al. [24] investigated the durability of the highly homogenized $Ti_8Cr_{12}V_{80}$ by floating zone melting and found that the desorption capacity of high V content $Ti_8Cr_{12}V_{80}$ alloy only decayed by 1.4% after 500 cycles, which was smaller than for the $Ti_{24}Cr_{36}V_{40}$ alloy. However, the price of metal vanadium is the most expensive among V–Ti-based solid solution alloys, so it is also meaningful to reduce the metal V content of the alloy on the basis of not affecting the performance of hydrogen storage alloys. Wang et al. [60] reported that the low-V suction-cast alloy rod $(Ti_{0.46}Cr_{0.54})_{95}V_5$ had a maximum hydrogen uptake of 3.14 wt% at 333 K, but the actual reversible hydrogen storage capacity was only about 2 wt%. Furthermore, the $(Ti_yCr_{1-y})_{95}V_5$ ($y = 0.38$–0.54) alloys have a relatively high reversible hydrogen storage capacity and a flat plateau only when the Ti/Cr ratio is close to the CN_{14} cluster [Ti_7Cr_8]. Furthermore, the incorporation of vanadium plays a crucial role in modulating both the plateau slope and hysteresis characteristics of hydrogen storage alloys [70, 90].

Table 1 Hydrogen storage properties of various V–Ti-based solid solution alloys

	Temperature (K)	P_{des} (MPa)	Reversible desorption capacity (wt%)	ΔS (J mol^{-1} K^{-1})	ΔH (kJ mol^{-1})	Refs.
$Ti_{27}Cr_{27}V_{40}Fe_6$	338	–	2.25	151.56	51.33	[12]
$Ti_{25}V_{40}Cr_{35}$	303	0.41	1.56	–	–	[42]
75V–Ti–15Cr–1Fe–1Al	298	0.5	2.26	–	–	[39]
$Ti_{24}V_{40}Cr_{34}Fe_2$	303	1.30	0.44	–	–	[42]
$Ti_{33}V_{37}Mn_{30}$	363	0.322	1.82	–	33	[40]
$Ti_{33}V_{37}Mn_{29.4}Ce_{0.6}$	363	0.124	1.98	–	43	[40]
$Ti_{16}Cr_{34}V_{50}$	293	–	2.24	–	–	[43]
$Ti_{16}Cr_{34}V_{49}Fe_1$	293	–	1.91	–	–	[43]
$Ti_{16}Cr_{30}V_{50}Nb_4$	303	–	2.21	–	–	[43]
$Ti_{25}Cr_{25}V_{25}Nb_5$	303	–	2.23	–	–	[43]
$Ti_{16}Zr_5Cr_{22}V_{55}Fe_2$	298		1.42	–	–	[46]
$(FeV_{80})_{48}Ti_{30}Cr_{26}$	298	0.2	2.0	–	–	[50]
$V_{40}Ti_{26}Cr_6Fe_8$	298	–	1.97	–	–	[49]
$(VFe)_{60}(TiCrCo)_{40}$	298	0.248	2.1	–	–	[64]
$(VFe)_{60}(TiCrCo)_{40}Zr_{0.5}$	298	0.189	2.0	–	–	[64]
$(Ti_{0.32}Cr_{0.43}V_{0.25})$ + 2 wt%La	293	–	2.23	–	–	[65]
$Ti_{12}Cr_{23}V_{65}$	295	–	2.5	–	–	[66]
$Ti_{12}Cr_{23}V_{65}Fe_1$	273	–	2.42	–	–	[66]
$TiCr_{1.2}(FeV)_{0.4}$	318	–	1.36	–	–	[72]
$V_{30}Ti_{32}Cr_{32}Fe_6$	373	–	2.56	–223.6	–40.8	[73]
75 at%V–5 at%Ti–Cr	273	0.35	2.3	–	–	[70]
$Ti_{10}V_{77}Cr_6Fe_6Zr$	333	0.75	1.82	–	–	[74]
$Ti_{27.25}Cr_{28.05}V_{37.25}Fe_{7.45}Ce_{1.0}$	343	–	2.25	–126.91	–41.97	[75]
$Ti_{32}Cr_{46}V_{22}Ce_{0.4}$	298	–	2.0	118	34.3	[76]
$(V_{30}Ti_{35}Cr_2Fe_{10})_{97.5}Si_{2.5}$	298	0.22	1.22	–	–	[77]
$(V_{30}Ti_{35}Cr_2Fe_{10})_{99.68}Si_{0.32}$	298	0.078	1.96	–	–	[77]
$V_{60}Ti_{22.4}Cr_{5.6}Fe_{12}$	298	0.062	2.12	–	–	[78]
Ti–28V–15Mn–10Cr	353	–	2.45	–	–	[79]
$Ti_{25}Cr_{50}V_{25}$	273	–	2.30	–	–	[80]
$Ti_{25}Cr_{49}V_{25}Fe_1$	273	–	1.96	–	–	[80]
$Ti_{25}Cr_{49}V_{25}Nb_1$	273	–	2.38	–	–	[80]
Ti–25V–10Cr–25Mn	353	0.21	2.44	–	–	[81]
Ti–10Cr–18Mn–27V–5Fe	333	2.42	2.0	–	–	[82]
60 at%V–15 at%Ti–25 at%Cr	353	0.0101	2.62	–	–	[83]
$Ti_{25}Cr_{50}V_{25}$	298	0.4	2.4	–	–	[84]
$Ti_{25}Cr_{50}V_{20}Mo_5$	298	2.3	2.4	–	–	[84]
$V_{35}Ti_{35}Mn_{30}$	303	0.054	1.18	–	–	[85]
$Ti_{0.5}V_{0.5}Mn$	260	–	1.9	–	–26.8	[86]
$Ti_{1.5}Mo_{0.5}CrV$	298	–	2.23	–	49.14	[87]
$V_{0.60}5Ti_{0.20}Cr_{0.12}Mn_{0.075}$	303	0.31	1.92	–	–	[88]
$(Ti_{0.267}Cr_{0.333}V_{0.40})_{93}Fe_7Ce_{1.1}$	298	–	2.05	–	–	[89]
$V_{40}Ti_{23}Mn_{37}$	303	0.05	1.41	–	34.88	[90]
$Ti_{19}Hf_4V_{40}Mn_{35}Cr_2$	293	–	1.58	–	–	[91]
$Ti_{19}Hf_4V_{40}Mn_{37}$	293		1.95	–	47.39	[92]
$V_{48}Fe_{12}Ti_{15}Cr_{25}$	295	1.01	1.66	123.55	30.12	[93]
$V_{48}Fe_{12}Ti_{14}Cr_{25}Al_1$	295	0.92	1.46	113.24	28.02	[93]

https://doi.org/10.1007/s40820-025-01672-w

Table 2 Properties of individual elements for V–Ti-based solid solution alloys

Elements	Primary functions	Refs.
V	Increase the BCC phase proportion Improve cyclic durability Increase hydrogen desorption plateau pressure Modulate hysteresis and slope of PCT curves	[24, 70] [90]
Nb	Increase the effective hydrogen storage capacity Improve the cyclic durability	[43, 80]
La/Ce	Improve the flatness of plateau Decrease slope factor Increase the effective hydrogen storage capacity Improve the activation property Suppress the influence of impurities Homogenize the composition and microstructure Decrease hydrogen desorption plateau pressure	[40, 65] [75, 76] [89, 94] [95, 96] [97]
Zr	Improved activation performance Improve the cyclic durability Suppress the Ti-containing phase separation Decrease the hydrogen ab/desorption capacities Decrease hydrogen desorption plateau pressure Decrease hysteresis and slope factor	[41, 64] [98, 99] [100]
Cr	Decrease the unit cell Increase the incubation period Slower hydrogen absorption kinetics Decrease hydrogen desorption plateau pressure Decrease slope factor	[33, 81]
Fe	Decrease the cell unit Increase the desorption plateau pressure Improve the activation property Improve the cyclic durability Decrease the hydrogen storage capacities Reduce the hysteresis	[42, 43, 66, 80, 82, 101]
Mn	Increase the plateau pressure Improve the activation property Increase the effective hydrogen storage capacity	[85, 88, 102]
Mo	Increase the desorption plateau pressure Improve the cyclic durability Weak stability of dihydride Reduce the hysteresis	[84, 87]
Si	Decrease the lattice parameter Increase the plateau pressure Improve the activation property Decrease the hydrogen ab/desorption capacities	[77, 103]
Al	Increase the lattice parameters of the BCC phase Increase the hydrogen desorption plateau pressure Decrease the hydrogen storage capacities Decrease the desorption kinetics Inhibit the formation of γ phase (dihydride) Increase the plateau hysteresis	[51, 93] [104] [105] [106]
B	Decrease the hydrogen storage capacities Increase the plateau pressure	[61]
O	Decrease the hydrogen storage capacities	[107]

As an element with relatively strong hydrogen affinity, the Nb element can improve the cyclic durability without losing the effective hydrogen storage capacity of the V–Ti-based solid solution [80]. Towata et al. [43] compared the effect of Nb substitution on the hydrogen storage properties of V–Ti–Cr alloys. In the case of low-V $Ti_{25}Cr_{45}V_{25}Nb_5$ alloy, the first and 10th hydrogen storage capacities of the alloy were 2.23 and 2.10 wt%, while the 1st and 10th capacities of $Ti_{25}Cr_{50}V_{25}$ were 2.30 and 1.96 wt%, respectively, indicating that the cycle stability of the sample after Nb substitution was improved without sacrificing the effective hydrogen storage capacity (Fig. 3a). The same is true for low-V $Ti_{25}Cr_{45}V_{25}Nb_5$ alloy. However, high Nb content, such as $TiCrV_{0.45}Nb_{0.45}$ alloy, can also lead to a significant decrease in desorption capacity [109]. Silva et al. [110] investigated in detail the hydrogen absorption and dehydrogenation properties of Nb-doped $(TiVNb)_{85}Cr_{15}$ alloy and found that the hydrogenation process went through the steps as alloy ↔ BCC solid solution ↔ BCC intermediate hydride ↔ FCC dihydride, while the hydrogen absorption at lower hydrogen pressures reached 2 H/M. They also found that the H atoms were randomly distributed at the interstitial positions of the BCC and FCC structures rather than in a locally ordered state.

Zr substitution has been found to improve the hydrogen storage properties of V–Ti-based solid solution alloys [41, 98–100, 111, 112]. Suitable Zr substitution can improve the activation performance and reduce the lag loss, as well as increase the effective hydrogen storage capacity of the $Ti_{0.85}VFe_{0.15}$ alloy. Through a comparative analysis of the PCTs for $Ti_{0.85}VFe_{0.15}$ and $Ti_{0.85}V_{0.95}Fe_{0.15}Zr_{0.05}$, it was observed that the Zr-substituted system exhibited reduced hysteresis and a more uniform desorption plateau, which is essential for long-term stability [99]. For TiCrV alloy, Zr substitution led to a decrease in hydrogen absorption due to the formation of the $ZrCr_2$ Laves phase. However, the cyclic hydrogen absorption performance was improved due to the inhibition of TiH_2 phase separation [98]. The investigation further confirmed the improvement on the activation property and cyclic durability for Zr substitution [111]. The phase composition of $(VFe)_{60}(TiCrCo)_{40}$ alloy with Zr substitution comprises mainly a BCC main phase, C14 Laves phase, and CeO_2 phase. The C14 phase obviously contributed to the improvement of the activation performance, and the addition of Zr reduced the strain accumulation during the hydrogen ab/desorption cycle. With the increment of Zr addition, the cyclic durability also improved accordingly, but the hydrogen storage capacity also decreased. In a recent study by Wang et al., the activation of the $Ti_{50}V_{50}Cr_{25}$ alloy was greatly improved to reach 90% of the max hydrogen absorption capacity in just 230 s (Fig. 3b) by the addition of 7 wt% Zr, [113]. Zr can be used to refine V–Ti solid solution alloys with nano-eutectic structures. Zhang et al. [114] prepared $Ti_{40}V_{60-x}Zr_x$ ($x = 20$, 25, 30) hydrogen storage alloys with nano-eutectic structures by arc melting, in which the hydrogen absorption of $Ti_{40}V_{35}Zr_{25}$ alloy can reach 2.4 wt% in 10 min at 473 K with 1 MPa H_2. Owing to the large difference in atomic size between V and Zr, the alloy generates large elastic energy, which leads to the formation of a stable multiphase eutectic structure that provides a high-density phase interface and generates a "synergistic effect," providing active sites and paths for H_2 dissociation and diffusion, and thus promotes the improvement of the hydrogenation kinetics and hydrogen storage capacity, but the reversible hydrogen storage capacity (1.077 wt%) is unsatisfactory due to stable hydride formation. Liu et al. [115] added 10 wt% Zr_8Ni_{21} alloy to $Ti_{37}V_{40}Mn_{23}$ alloy by arc melting. Compared with the $Ti_{37}V_{40}Mn_{23}$ alloy without ZrNi added, the dehydrogenation kinetics of the prepared $Ti_{37}V_{40}Mn_{23} + 10$ wt% Zr_8Ni_{21} alloy at 303 K was significantly improved (Fig. 3c). It could release 2.15 wt% of hydrogen at 363 K and the dehydrogenation activation energy of the $Ti_{37}V_{40}Mn_{23} + 10$ wt% Zr_8Ni_{21} alloy decreased to 55.20 kJ mol^{-1}. Kamble et al. [116] compared the effect of introducing Zr through different methods on the hydrogen storage properties of TiCrV alloys and found that the introduction of 4 wt% Zr into $Ti_{52}V_{12}Cr_{36}$ alloy by arc melting significantly improved the kinetic properties of the alloy wih a hydrogen storage capacity of up to 3.6 wt%, whereas the kinetic properties deteriorated when Zr was introduced through ball milling, and the authors attributed this phenomenon to the fact that ball milling only dispersed Zr on the surface of the particles that cannot form a ternary phase with Ti, Cr, and V.

It is recognized that the addition of rare earth elements can effectively improve the activation properties of alloys [65, 89, 95–97]. Singh et al. [65, 95] found that the La element has the best effect by comparing the effects of La, Y, Ce, and $LaNi_5$ on the hydrogen storage properties of V–Ti–Cr alloys. Although only 91% of the BCC phase involved in the dehydrogenation process, the $Ti_{0.32}Cr_{0.43}V_{0.25} + 5$ wt% La composite exhibited a desorption capacity of 2.31 wt% at 293 K and a flatter plateau after La substitution, as shown in

 https://doi.org/10.1007/s40820-025-01672-w

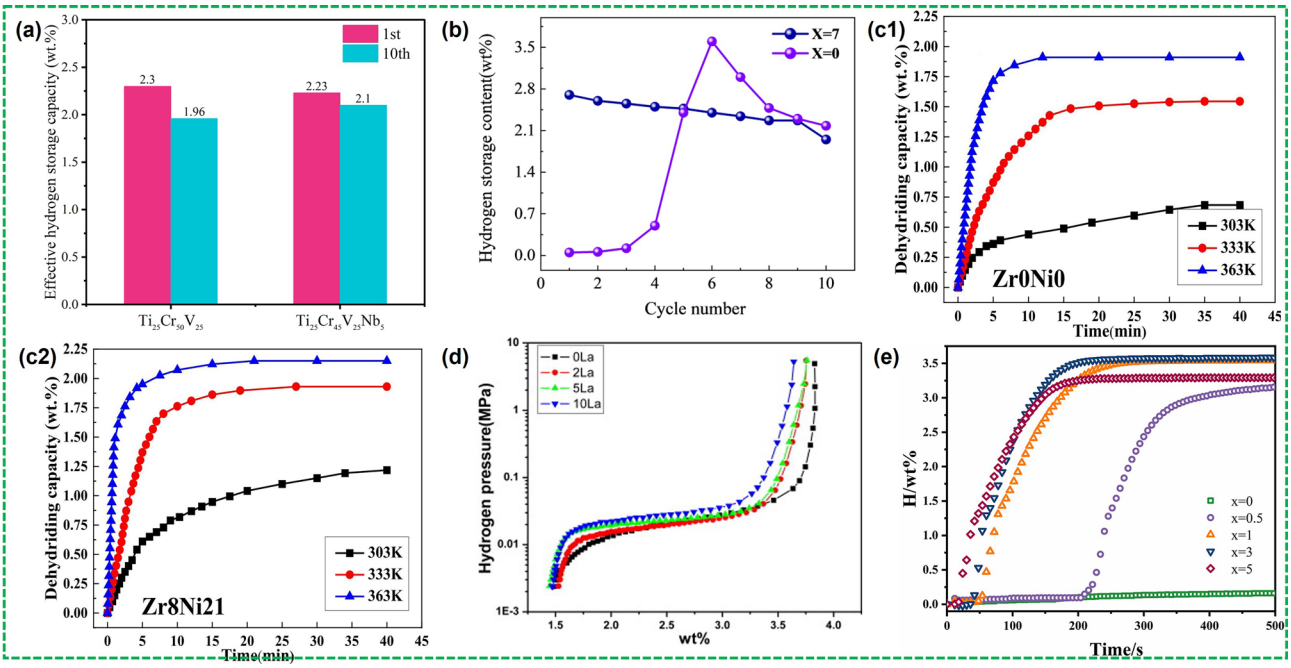

Fig. 3 **a** Effective hydrogen storage capacity of $Ti_{25}Cr_{50}V_{25}$ and $Ti_{25}Cr_{45}V_{25}Nb_5$ after 1st and 10th cycle. Reproduced with permission from Ref. [43]. Copyright 2013 Elsevier **b** Hydrogen capacities of $Ti_{50-x}V_{25}Cr_{25}Zr_x$ ($x=0$ and 7) alloys over 10 cycles at 303 K. Reproduced with permission from Ref. [113]. Kinetics curves of hydrogen desorption of $Ti_{37}V_{40}Mn_{23}+10$ wt% Zr_xNi_y alloys: **c1** Zr_0Ni_0 and **c2** Zr_8Ni_{21}. Reproduced with permission from Ref. [115]. Copyright 2024 Elsevier **d** Desorption P–C isotherms at 293 K for $(Ti_{0.32}Cr_{0.43}V_{0.25})+x$ wt% La ($x=0$, 2, 5, 10). Reproduced with permission from Ref. [65]. Copyright 2024 Elsevier **e** First hydrogen absorption kinetics of the $Ti_{28}Cr_{26}V_{35}Fe_6Mo_5+x$ wt% Y ($x=0$, 0.5, 1, 3, 5) alloys. Reproduced with permission from Ref. [120]. Copyright 2024 Elsevier

Fig. 3d. It should be noted that there is no significant reduction in effective hydrogen storage capacity, and the slope of the plateau was markedly diminished, which is positive for practical applications. In addition, Ce substitution with a suitable content can effectually homogenize the BCC phase, which reduces the oxygen concentration and suppresses the Ti-containing second phase separation, facilitating a more gradual plateau [89]. Due to the effective properties of deoxygenation, Ce element is often added to remove impurity elements in FeV master alloys. Liu et al. [76] studied the effect of Ce addition on hydrogen storage performance of $Ti_{32}Cr_{46}V_{22}$ alloy, and the results showed that Ce addition effectively improved the desorption plateau pressure and effective hydrogen storage capacity of the $V_{32}Cr_{46}V_{22}$ alloy. Notably, the slope of the plateau experienced a significant reduction. Chen et al. [40]. found that the BBC phase abundance of Ti–V–Mn alloys increased with the increase of Ce content, thus achieving a higher reversible hydrogen storage capacity. And Ce or $CeH_{2.51}$, rather than CeO_2, played a key role in the activation process, which had a more important effect than the C14 Laves phase in V–Ti-based solid solution alloys [40, 97].

At present, there are few studies on Sc and Y substitution. In Kwon et al.'s report [117], moderate Sc substitution achieved a higher hydrogen storage capacity than the original $Ti_{0.32}Cr_{0.43}V_{0.25}$ alloy, but the actual effective desorption capacity was reduced. In a separate study, however, it seemed that it had little effect on the improvement of the performance of 40Ti–40V–10Cr–10Mn alloys [118]. Excessive Sc substitution can result in the inability to embed into the BCC structure, while the generated ScH_2 can lead to a decrease in the effective desorption capacity at 373 K. By comparing the four $V_{35}Ti_{35}Cr_{10}Fe_{10}M_{10}$ (M = Mn, Co, Sc, or Ni) HEA alloys, Sc can indeed accelerate hydrogenation kinetics to a certain extent [119]. Chen et al. [120] introduced 1 wt% Y into the $Ti_{28}Cr_{26}V_{35}Fe_6Mo_5$ alloy and achieved better activation performance. After Y doping, the incubation period was reduced to 204 s (Y: 0.5 wt%) and below 50 s (Y: > 1 wt%), respectively (Fig. 3e). On the one hand, yttrium formed YH_2 during the hydrogenation process, providing a channel for H diffusion during activation.

On the other hand, the introduction of yttrium reduced the pulverization of the alloy. Liang et al. [121] introduced Y element into Ti–V–Mn alloy to prepare $Ti_{0.9}V_{1.1}Mn_{0.9}Y_{0.1}$ tetrameric alloy, which could absorb 3.54 wt% hydrogen in 3 min at room temperature and release 3.05 wt% hydrogen when dehydrogenated at 473 K until 1 bar, and the high reversible hydrogen storage capacity can be attributed to the coexistence of Y phase and C14 Laves phase.

In order to improve the weight hydrogen storage density of the alloy, Mariana et al. [122] prepared a $Mg_{35}Al_{15}Ti_{25}V_{10}Zn_{15}$ alloy by mechanical alloying under an argon atmosphere with Mg as the doping element, and the addition of Zn element was favorable for the formation of solid solution and avoiding the segregation of Mg. The prepared samples consisted of a BCC phase and a certain amount of unmixed Mg and could absorb 2.5 wt% hydrogen at 648 K and 4 MPa hydrogen pressure.

A small amount of Pd can also effectively improve the activation performance of $Ti_{33}V_{33}Cr_{34}$ alloy and improve its cycle stability [123]. However, Pd is even more expensive than metal V, making it difficult for practical application.

3.2.2 Hydrogen Labile Metal Substitution

V–Ti–Cr system is one of the most widely explored V-based alloys and the introduction of Cr improves the cyclic durability and powder resistance of V–Ti alloys without affecting their reversible hydrogen storage capacity, and the incorporation of Cr also facilitates a decrease in the plateau slope [81]. However, the long incubation time and the high temperature and high-pressure conditions required in the first activation process increase the manufacturing cost of the V–Ti–Cr alloys [33, 81]. The reason for the difficulty in activation is still inconclusive, but the oxide layer on the surface of the alloy is recognized as one of the culprits. To improve the activation properties of the V–Ti–Cr alloys, researchers have carried out plenty of research. Yu et al. [124] mixed quenched Ti–28V–15Mn–10Cr alloy with 10 wt% $LaNi_{3.55}Co_{0.75}Mn_{0.4}Al_{0.3}$ alloy by ball milling and found that the activation performance of the obtained composite was greatly improved, which was because the layer of $LaNi_{3.55}Co_{0.75}Mn_{0.4}Al_{0.3}$ on the surface of the alloy can effectively improve the diffusion and absorption of H. However, the effect of $LaNi_{3.55}Co_{0.75}Mn_{0.4}Al_{0.3}$ addition on other hydrogen storage properties was not given in this study.

For the V–Ti–Cr alloys, the effective hydrogen storage capacity and hydrogen desorption pressure of the alloys are mainly related to the Ti/Cr ratio and the V content [60, 70, 125–127]. When the Ti/Cr ratio is constant, the main phase of the alloys changes from Ti–Cr compounds to the BCC phase with the increase of V content. At the same time, the hydrogen storage performance of the alloys is greatly improved, but the activation performance becomes worse. Because H atoms diffuse more easily in Ti–Cr compounds with larger lattice constant, and the increase of the abundance of BCC phase raises H atom diffusion resistance [126]. The lattice parameters of the V–Ti–Cr alloys increase with the Ti/Cr ratio, which is not only related to the effective hydrogen storage capacity of the alloys but also associated with the cycle durability [33, 127]. Lin et al. [33] compared the cycling performance of V–Ti–Cr alloys with different Ti/Cr ratios, and the results show that the cycling durability of $Ti_{0.8}Cr_{1.2}V$ was better than TiCrV at various temperatures. Goshome et al. [128] investigated the performance of $V_{40}TiCr$ and $V_{70}TiCr$ as metal hydride hydrogen compressors and regulated the hydrogen absorption and desorption plateau of the alloys by varying the value of Ti/Cr, which in turn affects the hydrogen compression performance and cycling stability of the alloys. In order to reveal the occupancy of H atoms in V–Ti–Cr alloys, Sakaki et al. [129] used synchrotron radiation and neutron total scattering experiments to investigate the structure of the dihydride phases formed by $V_{10}Ti_{35}Cr_{55}$, $V_{50}Ti_{20}Cr_{30}$, and $V_{80}Ti_8Cr_{12}$ alloys, and the results show that the dihydride phases have an FCC structure in the whole and in the local area, and the crystal structure is CaF_2 structure, the interatomic distance between hydrogen and Cr is shorter than that with V, and the interatomic distance with Ti is longer than that with V, indicating that the hydrogen atoms do not occupy the centers of the tetrahedra but move toward the Cr atoms and away from the Ti atoms.

Fe element is also often introduced into the V–Ti-based solid solution alloys to improve the reversible hydrogen storage capacity of the alloys. For V–Ti–Cr alloys, Fe substitution will occupy Ti and Cr sites, resulting in a decrease in unit cell parameters and an increase in plateau pressure. As shown in Fig. 4a, Abdul and Chown prepared a series of Fe-doped $Ti_{35-0.5x}V_{40}Cr_{25-0.5x}Fe_x$ alloy and all Fe-doped alloys exhibited higher desorption plateau [42]. But the side effect of Fe substitution is also obvious, that is, the plateau becomes steeper, and the hydrogen storage capacity

 https://doi.org/10.1007/s40820-025-01672-w

decreases [42, 72, 101]. The effect of Fe substitution in the Ti–V–Mn system is different from that in the Ti–V–Cr system. Santos et al. [130] prepared a Ti–Mn–(FeV) solid solution alloy by replacing V with FeV alloy, which is equivalent to replacing vanadium with Fe in the Ti–V–Mn system. And the reversible hydrogen storage capacity of Ti–Mn–(FeV) alloy can be significantly increased despite the adverse effects of impurities in FeV alloy, which can be attributed to the fact that the desorption plateau pressure of V–Ti–Mn alloys is relatively low and the higher plateau pressure after Fe substitution is more favorable for hydrogen release. The Fe element also can improve the activation performance and cycle durability of V–Ti-based solid solution alloys [46, 66, 80, 82]. Hang et al. [46] obtained the $Ti_{16}Zr_5Cr_{22}V_{55}Fe_2$ alloy by partial substitution of Fe for V with BCC main phase and C14 secondary phase, which has good activation performance and exhibits an effective hydrogen storage capacity of 1.42 wt%. Aoki and Towata et al. [43, 66] focused on the effect of trace Fe on the cycle performance of Ti–Cr–V alloy and found that 1 at% Fe can significantly improve the cycle performance of the alloy. It is true that 1 at% Fe substitution slightly reduced the hydrogen storage capacity of the alloy from 2.50 to 2.42 wt%, but the capacity retention rate of $Ti_{12}Cr_{23}V_{64}Fe_1$ alloy after 100 cycles is 97%, while that of $Ti_{12}Cr_{23}V_{65}$ alloy is only 88% [66]. So, it seems worthwhile to sacrifice a tiny hydrogen storage capacity for a huge improvement in cycle durability. But for alloys with lower V content such as $Ti_{16}Cr_{34}V_{50}$ alloy, both the maximum hydrogen storage capacity and the effective hydrogen storage capacity will be greatly reduced after only adding 1 at% Fe [43]. If the amount of iron added is too high, even the high V alloy $Ti_{16}V_{60}Cr_{24}$, its effective hydrogen storage capacity will be significantly reduced [131].

Similar to V–Ti–Cr alloys, the phase structure of V–Ti–Mn alloy formed by Mn substitution is also related to the V content and the Ti/Mn ratio [85, 90, 102, 132]. Matsuda et al. [132] studied the effect of V content on the phase structure of V–Ti–Mn alloy and found that when the V content is greater than 40%, the alloy will only contain BCC phase; and when the V content is less than 26.7%, more than 90% of the alloy in the alloy phase is C14 phase. When the V content is constant, the proportion of the C14 phase in the alloys increases with the decrease of the Ti/Mn ratio. As mentioned in most literature, Mn substitution promotes the phase structure transformation of alloys from the BCC phase to the C14 phase. And the highly active C14 phase has good activation properties and can greatly shorten the incubation time of V–Ti–Mn alloys, as shown in Fig. 4b [102]. However, it will also lead to a significant decrease on the hydrogen storage capacity of the alloys because the C14 phase has a lower hydrogen storage capacity than the BCC phase [85, 88, 90, 102]. The lattice parameter of the BCC phase increases with the increase of the Ti/Mn ratio, which leads to an increase in the hydrogen absorption rate of the alloy, but the formed hydride is also more stable, making it difficult to dehydrogenate. Taghizadeh et al. [48] regulated the ratio of BCC phase and C14 phase in the alloys by remelting technique, which led to a decrease of BCC phase volume fraction, and the slope and hysteresis coefficient of the PCT curves decreased with increasing number of remelts. Recent studies by Hang et al. [133] have also shown that tiny Mn introduction can improve the flatness of the desorption plateau and plateau pressure of the $Ti_{16}Zr_5Cr_{22}V_{55-x}Fe_2Mn_x$ ($x = 0, 1, 2, 3$) alloys (Fig. 4b). It is a pity that the reversible hydrogen storage capacity of V–Ti–Mn alloys reported in the literature is mostly less than 2.0 wt% at ambient temperature (< 100 °C) [40, 85, 86, 134].

Mo can improve the plateau desorption pressure, the effective hydrogen storage capacity, and the cyclic durability of V–Ti-based solid solution alloys [84, 87]. Matsunaga et al. [84] studied the effect of Mo on the hydrogen storage properties of $Ti_{25}Cr_{50}V_{25}$ alloy and found that the dehydrogenation plateau pressure of $Ti_{25}Cr_{50}V_{20}Mo_5$ alloy at 298 K increased from 0.4 to 2.3 MPa after 5 at% Mo substitution, and the effective hydrogen storage capacity is still the original 2.4 wt% (Fig. 4d). Similar results were obtained by Hu et al. [87], the $Ti_{1.5}Mo_{0.5}CrV$ alloy exhibited a reversible hydrogen storage capacity of 2.33 wt% at 298 K, and the cycle durability was also greatly improved. This can be attributed to the decrease of dihydrides stability as well as the enthalpy change value (ΔH), and the hysteresis of dehydrogenation process is also significantly reduced. Recently, Lin et al. [135] studied the effect of Mo introduction on the cycling properties of low-V alloy $TiCr_{1.2}(V–Fe)_{0.6}$, and they believed that the introduction of Mo can effectively inhibit the formation of the second phase during the cycling process.

In addition, V–Ti-based solid solution alloys substituted with other metal elements, such as Hf [91, 92], and Rh [136] have also been extensively studied to improve the hydrogen storage performance of the alloys. The highest desorption capacity of 1.88 wt% at 293 K was achieved for the Hf

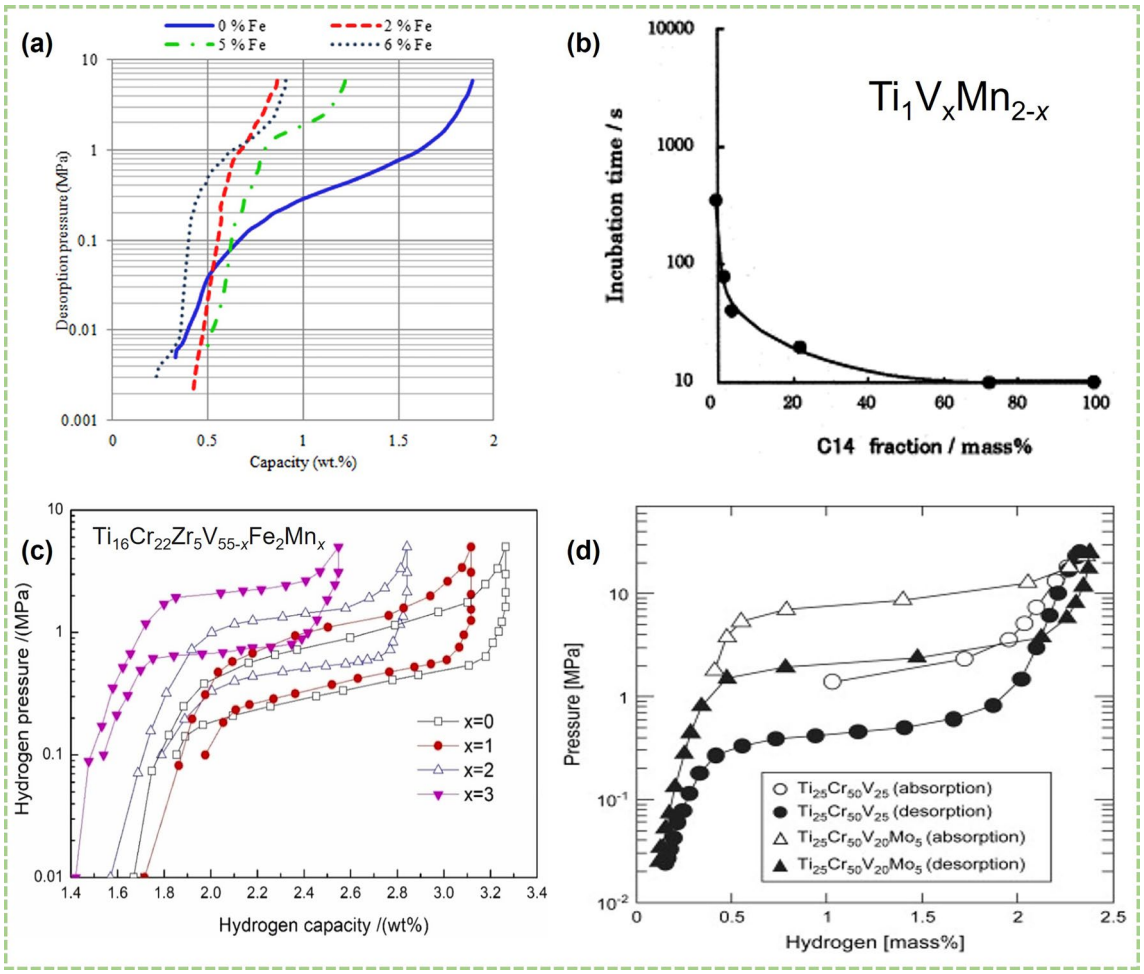

Fig. 4 **a** Effect of Fe on H desorption in $Ti_{25-0.5x}V_{40}Cr_{35-0.5x}Fe_x$ ($x=0$, 2, 5, 6 at%) alloys. Reproduced with permission from Ref. [42]. Copyright 2016 Elsevier **b** Relation between C14 phase fraction and incubation time. Reproduced with permission from Ref. [102]. Copyright 2002 Elsevier **c** PCT curves of $Ti_{16}Cr_{22}Zr_5V_{55-x}Fe_2Mn_x$ ($x=0$–3) samples at 298 K. Reproduced with permission from Ref. [133]. Copyright 2024 Elsevier **d** PC isotherms of TiCrV and TiCrVMo. Reproduced with permission from Ref. [84]. Copyright 2009 Elsevier

substituted-$Ti_{23}V_{40}Mn_{37}$ alloy. In addition, V–Ti–Ni alloys are mainly used in hydrogen separation/purification and Ni-MH batteries, which will not be repeated here.

At present, V–Ti-based solid solution alloys have been developed in the direction of multi-alloying, such as quaternary and quinary alloys, to meet the needs of different application scenarios with high effective hydrogen storage capacity, suitable plateau pressure, and lower dehydrogenation temperature, etc. Yoo et al. [67] studied the effect of the simultaneous substitution of Cr by Mn and Fe on the hydrogen storage properties of the Ti–Cr–V alloy. Not only the reversible hydrogen storage capacity of the prepared $Ti_{0.32}Cr_{0.32}V_{0.25}Fe_{0.03}Mn_{0.08}$ alloy at 293 K was increased from 2.3 to 2.5 wt%, but also the desorption plateau pressure was improved, while Mn substitution alone almost made plateau pressure no significant elevation. Zhu et al. [137] also confirmed the synergistic effect of Nb, Fe, Co, Ni, and Mn elements in improving the hydrogen storage properties, and $TiCrV_{0.7}(Nb_{0.2}Fe_{0.2}Co_{0.2}Ni_{0.2}Mn_{0.2})_{0.2}$ alloy had excellent hydrogen storage properties. It is also important to note that the activation performance of the alloy is crucial for on-board hydrogen storage devices. Because the difficulty of activation determines whether the process can be achieved in the MH tank. Several studies focusing on activation properties have also been carried out [138, 139]. The reduction of alloy particle size would help to reduce the difficulty of alloy activation, but the introduction of the second phase had a

 https://doi.org/10.1007/s40820-025-01672-w

more obvious effect on the improvement of alloy activation performance [138].

Multi-component high-entropy alloys (HEAs) are the current research hotspot [68, 140, 141] and their unique crystal structures directly mean that they have hydrogen storage properties that are different from conventional alloys, and they can be precisely modified by appropriate design, including chemical composition, crystal structure, valence electron concentration or lattice distortion parameters, and so on. The entropy characteristics of high-entropy alloys diverge significantly from those of traditional alloys. The total mixing entropy encompasses configurational entropy (ΔS_{mix}^{conf}), vibrational entropy (ΔS_{mix}^{vib}), magnetic dipole entropy (ΔS_{mix}^{mag}), and electronic randomness entropy (ΔS_{mix}^{elec}). The mixing entropy is dominated by configurational entropy. Li et al. believe that there is a certain relationship between valence electron concentration and hydrogen storage capacity for $V_{35}Ti_{35}Cr_{10}Fe_{10}M_{10}$ (M = Mn, Co, Sc, and Ni) alloys, and when valence electron concentration exceeded 5.17, hydrogen storage capacity began to decrease [119]. Ma et al. [142] prepared a TiVZrNbFe HEA by vacuum arc melting, which could absorb 1.60 wt% hydrogen at 323 K and 1 MPa for only 100 s. These results are similar to those of the TiZrFeMnCrV HEA [68] and have excellent kinetic properties. Recently, Serrano et al. [143] designed three HEAs with the alloy compositions of $Ti_{35}V_{35}Nb_{20}Cr_5Mn_5$, $Ti_{32}V_{32}Nb_{18}Cr_9Mn_9$, and $Ti_{27.5}V_{27.5}Nb_{20}Cr_{12.5}Mn_{12.5}$ by using the CALPHAD method. These HEAs absorbed hydrogen to form FCC hydrides with hydrogen storage capacities of 2.47, 2.09, and 3.38 wt%, respectively, and possessed excellent activation properties. The introduction of Cr and Mn promoted the formation of the AB_2-type Laves phase, which lowered the stability of the hydrides and facilitated the desorption of the hydrides. Balcerzak et al. [140] developed a low-crystallinity TiVFeCuNb HEA in accordance with the criteria established for single-phase high-entropy alloys ($\Delta S_{mix}^{conf} \geq 1.61\ R$; -15 kJ mol^{-1} $< \Delta H_{mix} < -5$ kJ mol^{-1}; $\delta r < 6.6\%$; $\Omega > 1.1$, where R is a gas constant), and the test results showed that the alloy had excellent kinetic properties and could reach half of its hydrogen storage capacity within 20 s. Regrettably, the maximum hydrogen storage capacity of the alloy is only 0.6 wt%. In addition, HEA can also be used as dopants for V–Ti-based solid solution alloys to improve the hydrogen storage properties of the alloys. Zhu et al. [137] provided a composite (high-entropy) doping strategy to prepare a low-cost $TiCrV_{0.7}(Nb_{0.2}Fe_{0.2}Co_{0.2}Ni_{0.2}Mn_{0.2})_{0.2}$ alloy (Fig. 5a). Compared with with single element substitution, the $TiCr_{1.0}V_{0.7}(HEA1)_{0.2}$ alloy displayed excellent activation properties (Fig. 5b). After heat treatment, the $TiCr_{1.0}V_{0.7}(HEA1)_{0.2}$ alloy could release 2.21 wt% H_2 cutting-off at 1 atm at 70 °C after fully absorbing hydrogen at lower temperature of 25 °C (Fig. 5c). Preparation of single-phase HEAs is an important task to improve reversiable hydrogen storage capacity [69, 144–151]. Montero et al. [149] prepared a single-phase $Ti_{0.30}V_{0.25}Zr_{0.10}Nb_{0.25}Ta_{0.10}$ HEA with a hydrogen storage capacity of up to 2.5 wt%, which remained at 2.2 wt% after 10th hydrogen absorption and desorption cycles. Recently, Chen et al. doped 1 at% Ce into V–Ti–Cr–Mn–Mo alloy to form a BCC-type Ti–Cr–V–Mn–Mo–Ce HEA (Fig. 5d). This stratagy resulted in a shorter incubation period of 40 s and a significant decrease of ΔH from 46.89 to 17.96 kJ mol^{-1} for the alloy (Fig. 5e). Although the introduction of Ce element reduced the hydrogen desorption plateau, the HEA-14-1-A alloy still achieved an effective improvement of hydrogen desorption capacity from 1.10 to 2.50 wt% (Fig. 5f) [152]. Many researchers have sought to prepare single-phase HEAs based on thermodynamic modeling [153–156] and experimentally to verify the correctness of the theory. Rapid quenching of melt is considered to be an effective method for the preparation of single-phase HEAs [157].

3.3 Heat Treatment

Heat treatment directly affects the hydrogen storage properties of the alloys due to the homogenization of the composition and the transformation to the structure that occurs during the process. Exactly, heat treatment in most cases means heat treating at a certain temperature for a period of time and then quenching in water in this review [74, 76, 84, 94, 158–160]. Table 3 summarizes the heat treatment conditions carried out for some V–Ti solid solution alloys and the corresponding phase structures. As shown in Fig. 6a, heat treatment may cause phase transformation, mainly between BCC and Laves phases. In general, the hydrogen storage capacity of BCC phase is higher than

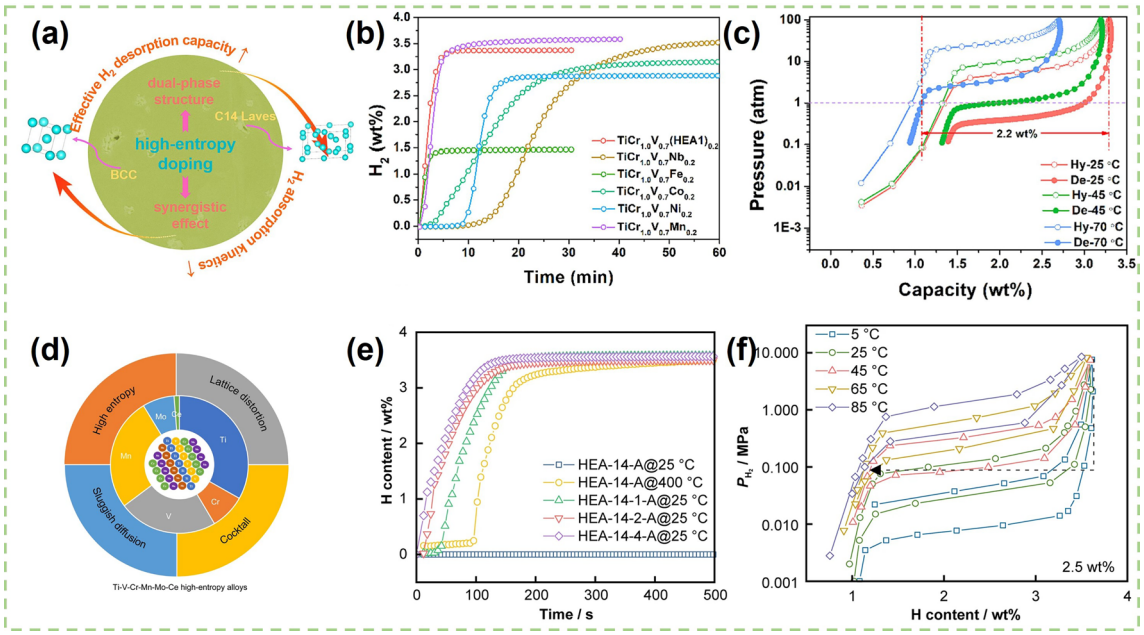

Fig. 5 **a** Schematic diagram of compositionally complex (high-entropy) doping strategy. **b** Hydrogen absorption kinetics of different alloys at 25 °C and 3 MPa H_2. **c** De-/hydrogenation PCT curves of heat-treated $TiCr_{1.0}V_{0.7}(HEA1)_{0.2}$ alloy at different temperatures. **a**–**c** Reproduced with permission from Ref. [137]. Copyright 2023 Elsevier **d** Schematic diagram of Ti–V–Cr–Mn–Mo-Ce high-entropy alloys. **e** First hydrogen absorption kinetics of HEAs after activation at different temperatures. **f** PCT curves of HEA-14-1-A alloys at different temperatures. **d**–**f** Reproduced with permission from Ref. [152]. Copyright 2024 Springer Nature

that of Laves phase, but the Laves phase is easier to activate than the BCC phase (Fig. 6b). Therefore, a satisfactory alloy always achieves a delicate balance between the two.

On the one hand, heat treatment promoted the conversion of the second phase to the BCC phase and increased the effective dehydrogenation capacity of the alloys under certain conditions [73, 74, 76, 117, 160]. The as-cast $V_{30}Ti_{32}Cr_{32}Fe_6$ alloy with BCC and C14 Laves phases changed into a single BCC phase after heat treatment at 1673 K for 30 min, which contributed to the increase of hydrogen storage capacity from 2.1 to 2.35 wt% at 298 K [73]. Liu et al. [165] compared the BCC phase abundance of as-cast and heat-treated $Ti_{19}Hf_4V_{40}Mn_{35}Cr_2$ alloys, and found that the BCC phase abundance of the heat-treated $Ti_{19}Hf_4V_{40}Mn_{35}Cr_2$ alloys was higher than that of the as-cast alloy (Fig. 6c). Both the C14 phase and the $ZrCr_2$ phase in the $Ti_{0.16}Zr_{0.05}Cr_{0.22}V_{0.57}$ alloy disappeared after heat treatment [160]. Hang et al. [74] systematically investigated the influence of different heat treatment conditions on microstructure and hydrogen storage properties of the $Ti_{10}V_{77}Cr_6Fe_6Zr$ alloy and found that the phase abundance of BCC annealed at 1523 K for 5 min effectively increased and the lattice strain decreased, leading to the increase of actual reversible hydrogen storage capacity. But heat treatment sometimes can also lead to an increase in the phase abundance of the C14 phase. For example, the proportion of the C14 phase increased in $V_{35}Ti_{20}Cr_{45}$ and $Ti_{42.75}Zr_{27}Mn_{20.25}V_{10}$ alloys after a heat treatment at 973 K for 72 h and 1173 K for 20 h respectively, which resulted in easier activation of the alloys [158, 163]. Figure 6d shows the microstructure of as-cast and heat-treated $Ti_{42.75}Zr_{27}Mn_{20.25}V_{10}$ alloys, which can be visually seen the increase of the Laves phases (C14 type). Luo et al. [162] also found that the effective hydrogen storage capacity of $V_{48}Fe_{12}Ti_{15}Cr_{25}$ alloy decreased after annealing although the hydrogen absorption and desorption kinetics were accelerated. Actually, the generation of the C14 phase after heat treatment improves the activation properties of the alloys. The reason for the two distinct phenomena may be that the BCC phase is stable at higher temperatures, whereas the Laves phase is not. High temperature and short time of heat treatment are more favorable to obtain BCC phase alloys.

 https://doi.org/10.1007/s40820-025-01672-w

Table 3 Heat treatment conditions and corresponding phase structures of some V–Ti-based solid solution alloys

Alloys	Heat treatment		Phase composition	Refs.
	Temperature (K)	Time (min)		
Ti–35V–45Cr	1573	1	BCC + secondary phase	[161]
Ti–10V–55.4Cr	1573	1	BCC + C14 Laves	[161]
Ti–5V–57.5Cr	1673	60	BCC + C14 Laves	[161]
$V_{30}Ti_{32}Cr_{32}Fe_6$	1673	30	BCC	[73]
$V_{0.605}Ti_{0.20}Cr_{0.12}Mn_{0.075}$	1573	480	–	[88]
$V_{48}Fe_{12}Ti_{15}Cr_{25}$	1273	600	BCC + Ti–rich + TiFe	[162]
$T_{32}Cr_{46}V_{22}Ce_{0.4}$	1673	5	BCC + CeO_2	[76]
$V_{35}Ti_{20}Cr_{45}$	973	4320	BCC + C14 Laves	[158]
$Ti_{31}V_{33}Cr_{19}Mn_{15}$	1473	600	–	[159]
$Ti_{0.16}Zr_{0.05}Cr_{0.22}V_{0.57}$	1473	480	BCC	[160]
$Ti_{0.95}Zr_{0.05}V_{0.2}Mn_{1.3}$	1173	4320	BCC	[44]
$Ti_{42.75}Zr_{27}Mn_{20.25}V_{10}$	1173	1200	BCC + C14 Laves	[163]
$Ti_{10}V_{77}Cr_6Fe_6Zr$	1573	5	BCC + C14 Laves	[74]
$Ti_{25}Cr_{50}V_{20}Mo_5$	1473	120	BCC	[87]
$Ti_{0.32}Cr_{0.39}V_{0.25}Sc_{0.04}$	1523	480	BCC	[117]
$(Ti_{0.267}Cr_{0.333}V_{0.40})_{93}Fe_7Ce_{1.1}$	1673	5	BCC + CeO_2/Ce	[89]
TiCrVMo	1473	120	BCC	[84]
$Ti_{26.5}Cr_{20}(V_{0.45}Fe_{0.085})_{100}Ce_{0.5}$	1673	5	BCC + secondary phase	[104]
$Ti_{24}Cr_{17.5}V_{50}Fe_{8.5}Ce_1$	1673	5	BCC + CeO_2	[94]
$Ti_{24}Cr_{36}V_{40}$	1673	180	–	[164]
$Ti_{0.5}V_{0.51}Mn$	1233	360	BCC + FCC + C14 Laves	[134]
$V_{40}Ti_{21.5}Cr_{38.5}$	1500	1440	BCC	[108]
$Ti_{25}Cr_{45}V_{25}Nb_5$	1600	10	BCC	[80]
$V_{60}Ti_{22.4}Cr_{5.6}Fe_{12}$	1673	30	BCC	[78]

On the other hand, heat treatment is shown to cause the plateau flatter by decreasing the lattice strain [73, 74, 76, 159, 160], as demnonstrated in Fig. 6e. Liu et al. [76] studied the effect of heat treatment on the plateau of BCC alloys and found the plateau was flatter than that of as-casted alloy after heat treatment. The $Ti_{32}Cr_{46}V_{22}$ alloy heat-treated at 1673 K for 5 min could desorb 1.75 wt% H_2 at 298 K and a pressure of 0.1 MPa, while the as-cast sample only released 1.35 wt% (Fig. 6f). There is no doubt that a flatter plateau is more conducive to hydrogen release. In the study conducted by Jeng et al. [159], the desorption plateau pressure of the $Ti_{31}V_{33}Cr_{21}Mn_{15}$ alloy increased from 1.43 to 2.33 atm after heat treatment at 1473 K for 10 h, and the slope factor decreased from 3.67 to 2.24 accordingly (Fig. 6g). The full width half maximum (FWHM) of the X-ray diffraction decreased, indicating that lattice strain was reduced after heat treatment, which was consistent with the change in the plateau slope factor [73, 76]. In addition, it can be seen from Fig. 6h that different heat treatment conditions have different effects on FWHM and the slope factor [74]. In brief, the change of effective hydrogen storage capacity of the alloys after heat treatment was influenced by the variation of phase structure and desorption plateau pressure.

Empirically, the temperature and duration of heat treatment need to be increased and prolonged respectively with the decrease of V content in the V–Ti–Cr alloys (Fig. 6i). Okada et al. [161] systematically investigated the effect of heat treatment on the phase structure and hydrogen storage performance of V–Ti–Cr alloys. For the Ti–35V–40Cr alloy, annealing above 1573 K was effective for flattening the plateau region and increasing the effective hydrogen storage capacity (Fig. 6j). For the Ti–10V–55.4Cr alloy, the C15 Laves phase could still be converted to BCC phase after annealing at 1573 K for 1 min (Fig. 6k). While the alloys with less than 10 at% V were more suitable to obtain more BCC phase at higher temperatures and longer

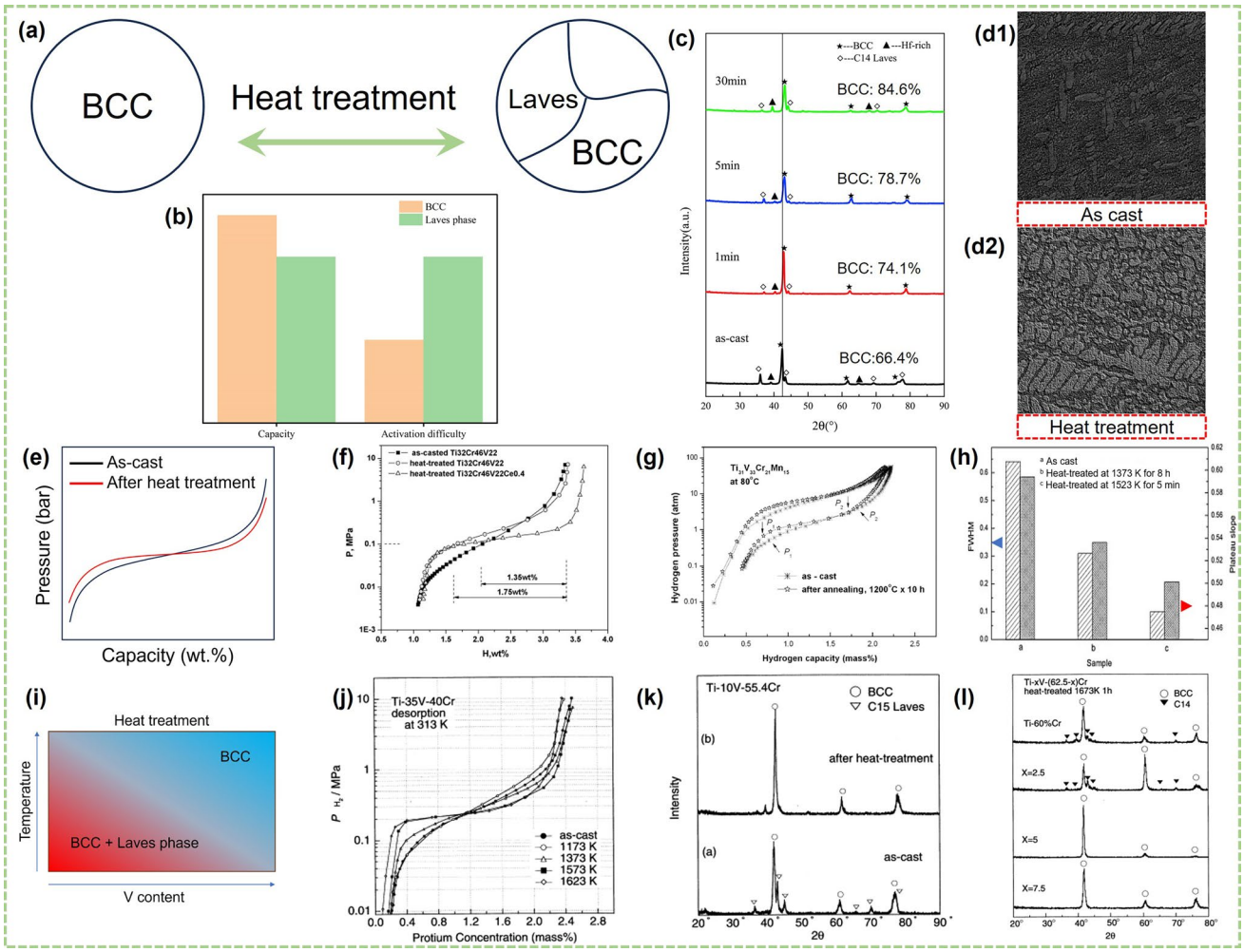

Fig. 6 **a** Schematic diagram of phase transformation caused by heat treatment. **b** Comparison of hydrogen storage capacity and activation difficulty of BCC phase and Laves phase. **c** XRD patterns and corresponding BCC phase abundance of as-cast and heat-treated $Ti_{19}Hf_4V_{40}Mn_{35}Cr_2$ alloys. Reproduced with permission from Ref. [165]. Copyright 2023 Elsevier Microstructure of $Ti_{42.75}Zr_{27}Mn_{20.25}V_{10}$ alloy: (**d1**) as-cast; (**d2**) after heat treatment at 900 °C. Reproduced with permission from Ref. [163]. Copyright 2021 Elsevier **e** Diagram of the effect of heat treatment on the PCT curves. **f** Dehydrogenation p–c isotherms of $Ti_{32}Cr_{46}V_{22}$ and $Ti_{32}Cr_{46}V_{22}Ce_{0.4}$ alloys at 298 K. Reproduced with permission from Ref. [76]. Copyright 2009 Elsevier g PCI results for $Ti_{31}V_{33}Cr_{21}Mn_{15}$ alloy before and after heat treatment. Reproduced with permission from Ref. [159]. Copyright 2011 Taylor&Francis. **h** The relationship between FWHM and desorption plateau slope of the as-cast and heat-treated samples: **a** as-cast; **b** heat-treated at 1373 K for 8 h; **c** heat-treated at 1523 K for 5 min. Reproduced with permission from Ref. [74]. Copyright 2012 Elsevier **i** Diagram of the effect of heat treatment temperature and V content on phase composition for V–Ti–Cr alloys. **j** P–C–T curves at desorption process of Ti–35V–40Cr alloys with a single b.c.c. phase annealed at 1173–1623 K for 2 h. **k** P–C–T curves at desorption process of Ti–35V–40Cr alloys with a single b.c.c. phase annealed at 1173–1623 K for 2 h. **l** XRD patterns of the Ti–*x*V–Cr ($x = 0$–7.5) alloys after a heat treatment at 1673 K for 1 h. **j–l** Reproduced with permission from Ref. [161]. Copyright 2002 Elsevier

periods of time (1673 K for 60 min), as shown in Fig. 6l. In other words, for the alloy with less V content, higher heat treatment temperature and longer duration time are needed to obtain more BCC main phase. Yu et al. [79] obtained a Ti–28V–15Mn–10Cr alloy with smaller grains quenched by a water-cooled rotating molybdenum disk, which induced the C14 phase to disappear and converted to the BCC phase during the component homogenization process. Under the condition of 353 K, the plateau of the quenched Ti–28V–15Mn–10Cr alloy was flatter than that of the as-cast sample, and the hydrogen storage capacity was also improved from 2.3 to 2.45 wt%. In addition, the prolongation of annealing time led to a further precipitation of the Ti–rich phase, and the Ti–35V–40Cr alloy annealed

 https://doi.org/10.1007/s40820-025-01672-w

at 1573 K for 1 min showed about 2.6 wt% hydrogen storage capacity, but the capacity decreased significantly after extending the annealing time to 50 h. The quenching treatment sometimes had an adverse effect on the V–Ti-based hydrogen storage alloys. For example, the first activation process after quenching becasme more difficult than the as-cast sample [79].

3.4 Degradation Mechanism

The degradation of capacity is affected by many factors, which can be divided into two categories, intrinsic factors and extrinsic factors. The intrinsic factors include element composition, particle size, micro-strain, dislocation density, and so on. Extrinsic factors mainly include impurity gas (O_2, H_2O, CO, etc.) and cyclic testing conditions. The attenuation of capacity is offen influenced by multiple factors superimposed on each other in practical applications.

The element composition of an alloy directly affects its cyclic properties. Generally, the high V alloys have better cycle stability than the low-V alloys [108]. Selvaraj et al. [108] found that the low-V alloy would undergo disproportionation during the cycles and a small fraction of Ti and V would be precipitated and subsequently converted into corresponding hydrides, which may be one of the reasons for the poor cyclic durability of low-V alloys. Kuriiwa et al. [70] gave detailed data on the effects of V content and Ti/Cr ratio on the cyclic properties of the alloy. As shown in Fig. 7a, both 80V–8Ti–Cr and 75V-5Ti–Cr alloys showed good cycle stability compared with the 60V–16Ti–Cr alloy. In addition, Ti/Cr ratio played a key role to obtain higher effective hydrogen capacity as well as good capacity retention rate. Recently, Yang et al. [166] compared the microstructures and hydrogen storage performances of three V contents alloys (20%, 40%, and 60%). The $V_{60}Ti_{19}Cr_{19}Fe_2$ alloy (V60) achieved better cycle stability than the $V_{40}Ti_{28.5}Cr_{30.1}Fe_{1.4}$ (V40) alloy (Fig. 7b). The authors believed that the smaller bulk elastic modulus due to the higher V content effectively reduced strain accumulation and volume expansion.

The micro-strain accumulated during cycles will distort lattice interstices and cumber or even prohibit the entry of hydrogen atoms, leading to a significantly degraded hydrogen capacity [111, 164]. Wu et al. [78] studied the hydrogen storage capacity and micro-strain changes of the $V_{60}Ti_{(21.4+x)}Cr_{(6.6-x)}Fe_{12}(0 \le x \le 3)$ alloys during hydrogen absorption and desorption cycles. The experimental results show that with the progress of hydrogen absorption and desorption, the reversible hydrogen storage capacity of the alloy was constantly attenuated. At the same time, its micro-strain was also increasing during ab/desorption cycles (Fig. 7c), and the macroscopic realization was a decrease in the desorption plateau pressure.

Zr substitution can reduce the micro-strain accumulation during the hydrogen ab/desorption cycles as well as Fe and Nb elements [66, 80, 111]. By comparing the changes of FWHM, Aoki et al. [66] found that Fe substitution inhibited the increase of lattice strain in the hydrogen ab/desorption cycles, thus greatly improving the cycle durability of $Ti_{12}Cr_{23}V_{64}Fe_1$ alloy, as shown in Fig. 7. A similar effect was also concluded in the work conducted by Yang et al. [111] which showed that the micro-strain increase of Zr-substituted $(VFe)_{60}(TiCrCo)_{40}$ alloy during hydrogen ab/desorption cycles was suppressed, and the capacity decay was only 4.5% after 10 cycles. Zr substitution, however, did not inhibit the growth of micro-srain in the alloy (Fig. 7d). There is no definitive explanation as to why the substitution of Fe, Nb, and Zr, etc. elements can reduce strain accumulation. In addition, annealing can effectively reduce dislocations in the Ti–Cr–V alloys but the dehydrogenation performance cannot be improved, because the dislocation accumulation mainly occurred in the hydrogen absorption process [164].

In addition, micro-strain is closely related to particle size. Luo et al. [167] investigated the decaying behaviors of the $V_{40}(TiCr)_{51}Fe_8Mn$ alloys with different particle sizes (60, 100, 200, 400, and 500 mesh) and found that the decay rate of dehydrogenation capacity decreased with the decreasing of alloy powder particle size (from 60 mesh down to 400 mesh). While the particle size was reduced to 500 mesh, the hydrogen storage properties of $V_{40}(TiCr)_{51}Fe_8Mn$ alloy deteriorated in all aspects (Fig. 7e). When the particle size of the alloy powder is blindly reduced, the hydrogen storage performance of the alloy will deteriorate. Kown et al. [168] found that the hydrogen storage capacity of the nano/micro-particle containing alloys decreased compared to that of the mechanically crushed particles from ingots (Fig. 7f). The reasons for this phenomenon have not yet been determined though there are several viewpoints focusing mainly in the following two points. One is that a smaller particle size makes the alloy powder easy to be poisoned by external factors, and the other is that an alloy powder with a smaller

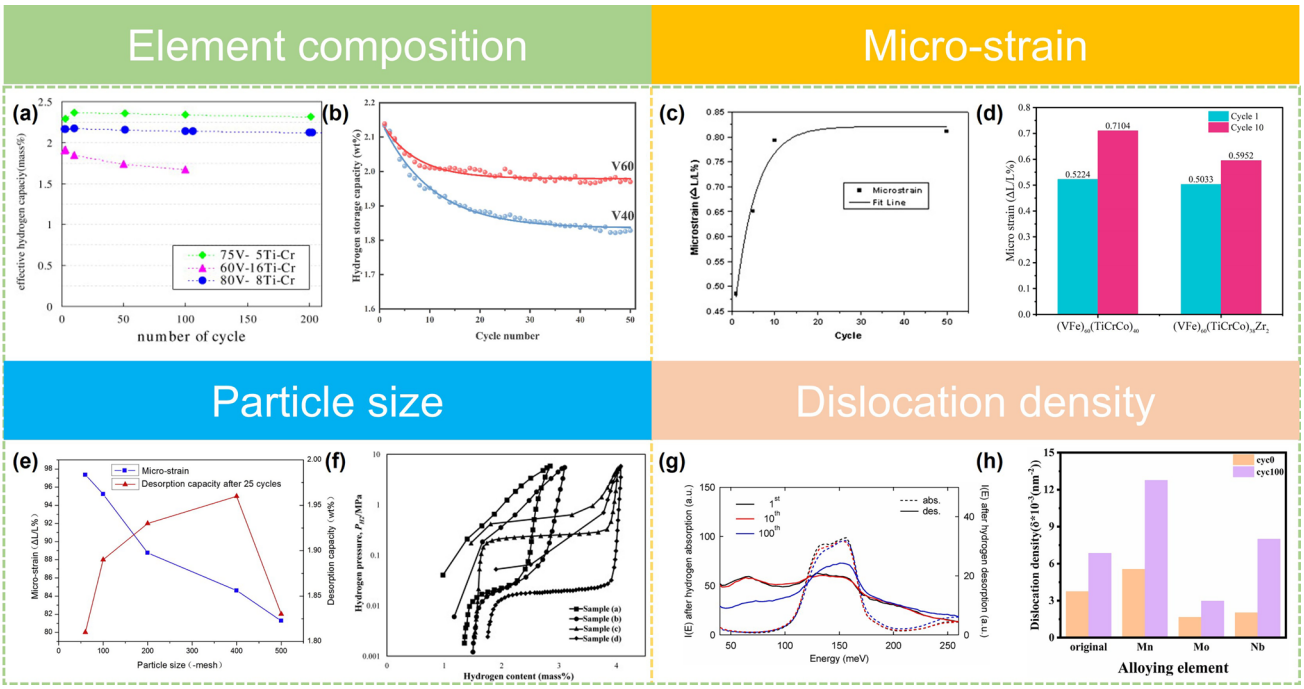

Fig. 7 **a** Relationship between effective hydrogen capacity and cycle number of 75at%V–5at%Ti–Cr as-cast sample along with those of 60at%V–16at%Ti–Cr and 80at%V–8at%Ti–Cr. Reproduced with permission from Ref. [70]. Copyright 2010 Elsevier **b** Hydrogen storage capacities of the V40 and V60 alloys at 333 K during cycling. Reproduced with permission from Ref. [166]. Copyright 2023 Elsevier **c** Fitting of micro-strain of $V_{60}Ti_{22.4}Cr_{5.6}Fe_{12}$ monohydride during absorption/desorption cycles. Reproduced with permission from Ref. [78]. Copyright 2010 Elsevier **d** Micro-strain of the $(VFe)_{60}(TiCrCo)_{40-x}Zr_x$ alloys ($x=0$, 2) after different hydrogen absorption–desorption cycles. Reproduced with permission from Ref. [111]. Copyright 2016 Elsevier **e** The relationship patterns of desorption capacity and micro-strain of $(VFe)_{48}(TiCrMn)_{52}$ alloy with different particle sizes after the 25th cycle. Reproduced with permission from Ref. [167]. Copyright 2015 Elsevier **f** P–C isotherms of the exploded particles with **a** composition #1, **b** composition #2 and the mechanically crushed particles from ingot with **c** composition #2, **d** composition #3 measured at 293 K. Reproduced with permission from Ref. [168]. Copyright 2012 Elsevier **g** Inelastic neutron scattering intensities, I(E), after hydrogen absorption and desorption of $V_{0.10}Ti_{0.36}Cr_{0.54}$. Reproduced with permission from Ref. [171]. Copyright 2024 Elsevier **h** Dislocation density of original alloy ($TiCr_{1.2}(V–Fe)_{0.6}$) and $TiCr_{1.1}M_{0.1}(V–Fe)_{0.6}$ (M = Mn, Mo, Nb) alloys before hydrogenation and after cycling. Reproduced with permission from Ref. [135]. Copyright 2024 Elsevier

particle size increases the specific surface area. Therefore, the sites for H atom occupancy are reduced, resulting in a decrease in the hydrogen storage capacity [167, 168].

Dislocation density is closely related to micro-strain and particle size. Kim et al. [169] investigated the origin of the capacity degradation of V–Ti-based solid solution alloys during cycling by using the atomic pair distribution function (PDF) analysis, and the results showed that the large number of dislocations generated in the alloys during cycling is closely related to the capacity fading. Ball milling often introduces defects and strain in the material. Wu et al. [170] observed that the hydrogen storage capacity of the $V_{60}Ti_{25}Cr_3Fe_{12}$ alloy decreased with the prolongation of milling time. Correspondingly, the strain and dislocation density in the alloys gradually increased during ball milling and make insuffient improvement of cycle stability. Recently, Ikeda et al. revealed that the degradation of hydrogen storage capacity stems from the introduced dislocations during the ab/desorption cycle by inelastic neutron scattering. The intensity at different energy (meV) represents different H-occupied sites of octahedral sites and tetrahedral sites. After 100 cycles, the inelastic neutron scattering intensities curves changed with a decrease in hydrogen at the octahedral sites and a similar increase at the tetrahedral sites, which is different from the both hydrogen occupation of tetrahedral and octahedral sites during the early cycles (Fig. 7g). Li et al. [135] explored the effect of adding different metal elements (M = Mn, Mo, Nb) on the capacity decay of $TiCr_{1.1}M_{0.1}(V–Fe)_{0.6}$ alloys, and they observed that the capacity retention rate of $TiCr_{1.1}Mo_{0.1}(V–Fe)_{0.6}$ alloy was the highest after Mo subsitition. It is found that both the grain size and micro-strain of the $TiCr_{1.1}Mo_{0.1}(V–Fe)_{0.6}$

 https://doi.org/10.1007/s40820-025-01672-w

alloys were increased after cycling, but the dislocation density of the alloy with Mo subsitition was the lowest after cycling (Fig. 7h), which might be the reason for its high capacity retention rate.

Some researchers have studied the capacity decay behavior of V–Ti-based hydrogen storage alloys in impure hydrogen. Generally, the influence of impurity oxygen atmosphere on pure V is greater than that of V–Ti alloys (Fig. 8a). The initial capacity of the $V_{40}Fe_8Ti_{26}Cr_{26}$ alloy decayed after four cycles in H_2 blended with 250 ppm of O_2, and the tolerance toward O_2 of the alloy could be improved effectively by loading a layer of metal La on the surface of the alloy through surface engineering, which can provide diffusion pathways due to the formation of diffusion-inhibiting oxides [172]. Unfortunately, no specific hydrogen storage capacity was given. Forming the second phase in the BCC matrix is an effective strategy to improve the toxicity resistance. Yu et al. [139] investigated the effect of ZnO addition on hydrogen storage performance of the Ti-30V-15Mn-15Cr alloy after air exposure, as shown in Fig. 8b. The alloy with the addition of 3 wt% ZnO decreased sensitivity to air exposure since ZnO acted as a hydrogen diffusion channel for hydrogen into the bulk alloy, making the alloy easy to absorb hydrogen. In another study by Yu et al. [82], the Fe-substituted Ti–10Cr–18Mn–27V–5Fe was more easily activated than iron–free Ti–10Cr–18Mn–32V alloy after air exposure, which can be attributed to the fact that the C14 phase generated after Fe substitution was more likely to be cracked and formed more channels for H diffusion. Recently, Xie et al. [173] repoted a Si-induced air-tolerant hydride to improve air-poisoning resistance of vanadium-based alloys. The $(V_{75}Ti_{11}Cr_{13}Fe_1)_{99}Si_1$ alloy can maintain about 85% of hydrogen absorption capacity after 10 cycles in $H_2 + 250$ ppm atmosphere, which can be contributed to the formation of $Ti_5Si_3H_{0.9}$ induced by 1 at% Si addition during hydrogen absorption cycles, as shown in Fig. 8c. The $Ti_5Si_3H_{0.9}$ played a role of hydrogen diffusion channel for the bulk. On the contrary, the Si-free $V_{75}Ti_{11}Cr_{13}Fe_1$ alloy almost lost the ability to absorb hydrogen under the same conditions. However, the addition of Si would inevitably reduce the reversible hydrogen storage capacity, which required a balance between toxic resistance and reversible hydrogen storage capacity. In addition, Suwarno et al. [33, 174] explored the possibility that the alloy could be reactivated after poisoning. When CO-containing gas was introduced during the hydrogen ab/desorption cycle, the hydrogen storage capacity would plummet. However, part of the hydrogen storage capacity would be restored when the CO-free hydrogen was re-introduced (Fig. 8d, e). This research, which can be defined as "waste alloy regeneration," contributed to the practical application of vanadium-based solid solution alloys.

The cycle conditions also affect the cyclic stability of the alloys to a certain extent. Lin et al. [175] reported the capacity durability of the $Ti_{0.8}Cr_{1.2}V$ alloy at different temperatures for dehydrogenation and found that the cycle durability worsened with the decrease in the dehydrogenation temperature (Fig. 8f). The β-phase formed during hydrogen absorption had high thermal stability, but its reversibility was poor, requiring higher dehydrogenation temperatures, thus leading to a reduction of its room-temperature cycling stability [6]. Recently, Wu et al. [176] proposed that the depth of dehydrogenation (DOD) also affected cycle stability, and the capacity decay rate was 4.37% at 40% DOD but rose to 8.74% at 100% DOD (Fig. 8g). In practical applications, too much reduction in the depth of dehydrogenation may effectively reduce micro-strain accumulation and volume expansion. The heating rate during desorption process may also affect the cyclic properties of the alloys. In the study of Suwarno et al. [33], the heating rate of 30 K min^{-1} led to the obvious attenuation of hydrogen storage capacity compared with the heating rate of 5 K min^{-1} (Fig. 8h). Therefore, where possible, the establishment of a uniform cycle test standard will help to compare the cycle stability of different alloys.

3.5 Some Issues of Using Industrial Grade V-Rich Alloy as a Raw Material for Large-Scale Applications

Due to the high costs of raw materials, especially for vanadium, replacing V with vanadium master alloy and using low-purity V are the main strategies to reduce the cost of preparing V-based alloys [50, 72, 73, 111, 130, 178]. There are many different types of industrial–grade vanadium alloys such as ferrovanadium (FeV) alloys, vanadium nitride (VN) alloys, and vanadium oxygen (VO) alloys (Fig. 9a). Among them, the residual B, C, N, O, Si, and Al, etc., in the raw metal vanadium or V alloys will have a key impact on the performance of the prepared V–Ti-based solid solution

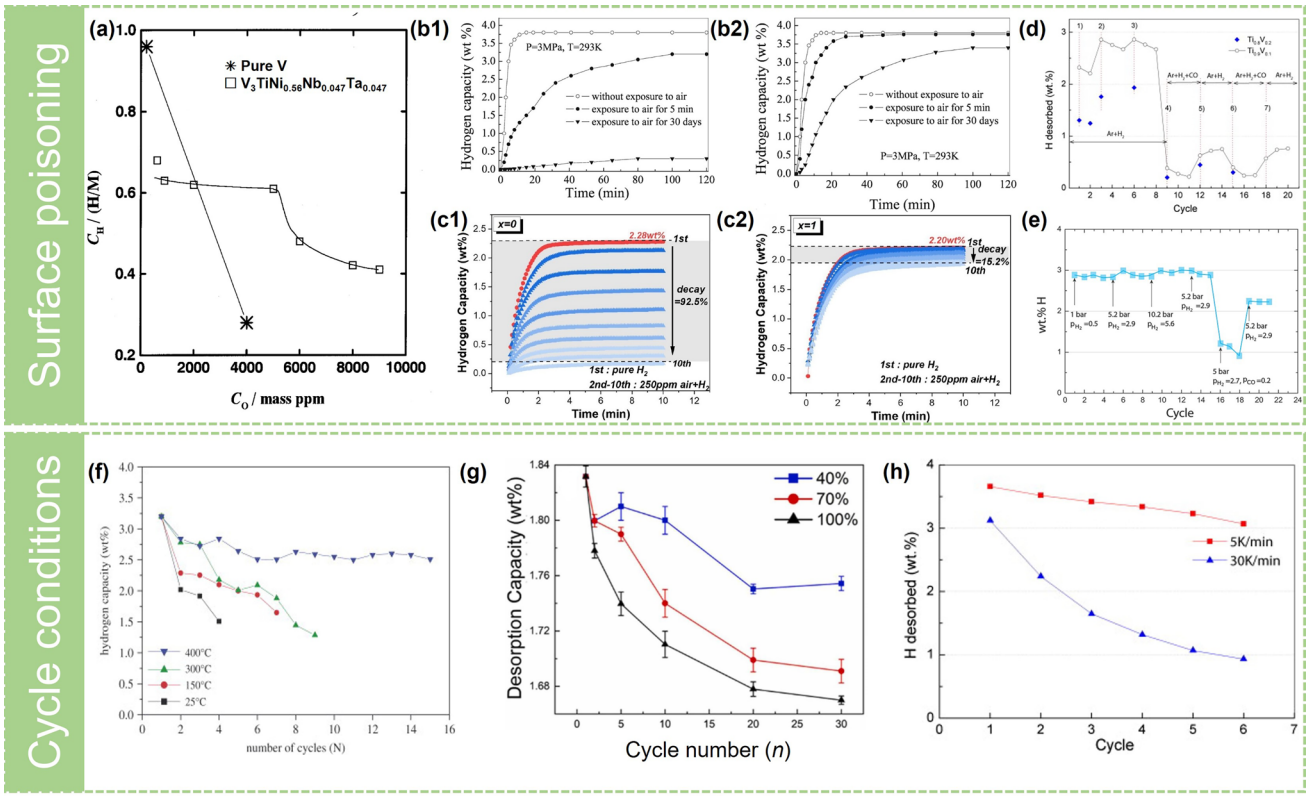

Fig. 8 **a** Effective hydrogen capacity C_H plotted against the oxygen concentration Co for the $V_3TiNi_{0.56}Co_{0.14}Nb_{0.047}Ta_{0.047}$ alloy in comparison with V. Reproduced with permission from Ref. [177]. Copyright 1998 Elsevier Hydrogen absorption curves of Ti–30V–15Mn–15Cr alloy powder with exposure to air for various durations: **b1** without nano ZnO and **b2** modified by 3 wt% nano ZnO. Reproduced with permission from Ref. [139]. Copyright 2004 Springer Nature. **c1** Hydrogen sorption cycling of the alloy $x=0$ in H_2+250 ppm air atmosphere and **c2** the alloy $x=1$ in H_2+250 ppm air atmosphere. Reproduced with permission from Ref. [173]. Copyright 2024 Elsevier **d** Amount of hydrogen desorbed during the TPR cycles. During hydrogen absorption, total gaseous pressure was 1 bar for both mixture I ($Ar+H_2$) and II ($Ar+H_2+CO$) with a flow rate of 50 mL min^{-1}. Hydrogen was absorbed during cooling to 200 °C and desorbed during heating of the samples to 700 °C with a rate of 30 K min^{-1} for both temperature increase and decrease. Composition of the mixtures during the absorption was as follows (1) $Ar+8\%H_2$, (2) $Ar+50\%H_2$, (3) $Ar+80\%H_2$, (4) $Ar+50\%H_2+5\%CO$, (5) $Ar+5\%H_2$, (6) $Ar+80\%H_2+2\%CO$, and (7) $Ar+8\%H_2$. Desorption conditions were chosen as: 1 bar Ar gas; flow rate 50 mL min^{-1}. Reproduced with permission from Ref. [33]. Copyright 2012 Elsevier **e** Reversible hydrogen storage capacity of $Ti_{0.9}V_{0.1}$ during hydrogenation and dehydrogenation cycling in the temperature range 150–780 °C, 5 deg min^{-1} cooling and heating rate. Hydrogenation was done at different hydrogen pressures, and dehydrogenation was done in pure Ar, 100 mL min^{-1} gas flow. CO was introduced into the gas flow before cycle 16 and removed after cycle 18. Reproduced with permission from Ref. [174]. Copyright 2016 Elsevier **f** Cyclic hydrogen capacities for the $Ti_{0.8}Cr_{1.2}V$ alloy at various temperatures. Reproduced with permission from Ref. [175]. Copyright 2007 Elsevier **g** Desorption capacity at different DOD. Reproduced with permission from Ref. [176]. Copyright 2023 Elsevier **h** Amount of hydrogen desorbed from the $Ti_{0.9}V_{0.1}$–based hydride formed during H absorption at 1 bar $Ar+8\%H_2$ at two different cooling rates, 5 and 30 K min^{-1}. Gas flow rate was 30 mL min^{-1}. Hydrogen desorption proceeded into Ar gas. Limiting absorption and desorption temperatures were 200 and 700 °C. Reproduced with permission from Ref. [33]. Copyright 2012 Elsevier

alloys [103, 178–181]. Ferrovanadium alloys have been the most studied in cost reduction possibilities for the preparation of V–Ti-based solid solution alloys. Fig. 9b shows the chemical composition requirements of different ferrovanadium alloys in international standard (ISO 5451:2022). The Chinese standards for ferrovanadium alloys provide more detailed criteria for composition control and different grades. Understanding the effect of impurity elements in ferrovanadium alloys on hydrogen storage properties is the key to prepare high-performance and low-cost V–Ti-based solid solution alloys.

One of the consequences of using ferrovanadium alloy instead of partial pure vanadium as raw material is that the incubation time of the first hydrogenation would be increased. Hout et al. [182] replaced 50% vanadium by ferrovanadium to prepare a low-cost V–Ti-based BCC alloy. As can be seen from Fig. 9c, the FeV substituted $Ti_{1.56}V_{0.18}(FeV)_{0.18}Cr_{1.08}+4\%Zr_7Ni_{10}$ alloy experienced a

 https://doi.org/10.1007/s40820-025-01672-w

longer incubation time during the first hydrogenation process than the unsubstituted $Ti_{1.56}V_{0.36}Cr_{1.08}+4\%Zr_7Ni_{10}$ alloy at 25 °C. The oxygen content in raw materials has a key effect on the hydrogen storage properties of V–Ti-based hydrogen storage alloys. For example, the elements with a higher affinity toward oxygen, e.g., Ti, would promote the formation of a Ti–rich secondary phase that led to an increase in the pressure of the plateau [107, 180]. Deoxidization can be achieved by the addition of La, Y, and Ce and further improve the flatness of plateau and enlarge the hydrogen capacity [75]. Mi et al. [75] prepared a low-cost V–Ti-based BCC alloy with commercial ferrovanadium and the $Ti_{27.25}Cr_{28.05}V_{37.25}Fe_{7.45}Ce_1$ alloy exhibited a faster first hydrogenation kinetics with 1 at% Ce added, as shown in Fig. 9d. In addition, Ce substitution was shown to improve the activation performance of the $Ti_{33}V_{37}Mn_{30}$ alloy due to the formation of $CeH_{2.51}$, and the hydrogen absorption capacity of the alloy increased with the increase of Ce content [40]. But unfortunately, the introduction of Ce led to the increase of the stability of the formed hydride, which resulted in a relatively high temperature needed to release H_2.

The effect of the Al element on the hydrogen storage properties of V–Ti-based alloys has been explored in many studies [39, 93, 104–106]. The $V_{48}Fe_{12}Ti_{15}Cr_{25}$ alloy exhibited a lower desorption kinetics performance and higher thermodynamic stability with 1 at% Al substitution [93]. Mi et al. [104] studied the effect of Al addition on the microstructures and hydrogen storage properties of $Ti_{26.5}Cr_{20}(V_{0.45}Fe_{0.085})_{100-x}Al_xCe_{0.5}$ ($x=0$, 0.5, 1.0, and 1.5 at%) alloys. They found that with the increase of Al content, the lattice parameters of the BCC phase, desorption plateau pressure and slope factor of the alloys increased, but the hydrogen storage capacity decreased. Ce is also a useful element to suppress the side effect of Al on the hydrogen storage performance of the Ti–V alloy, which could format the Al–Ce–O secondary phase. However, Wu et al. [39] reported that the simultaneous introduction of Al and Fe into the V–Ti–Cr alloy resulted in better hydrogen storage properties than only adding Fe or Al. They believe that Al preferentially occupies the position along *c* axis in the V-based solid solution alloy that leads to a decrease in the lattice parameter of *c*, while the addition of Fe will shorten the lattice parameter a but extend the c. The overall result is that the change in lattice volume would be canceled out.

Similarly, the Si element also adversely affects the hydrogen storage properties of V–Ti-based solid solution alloys [77, 103, 183]. Although Si addition could improve the

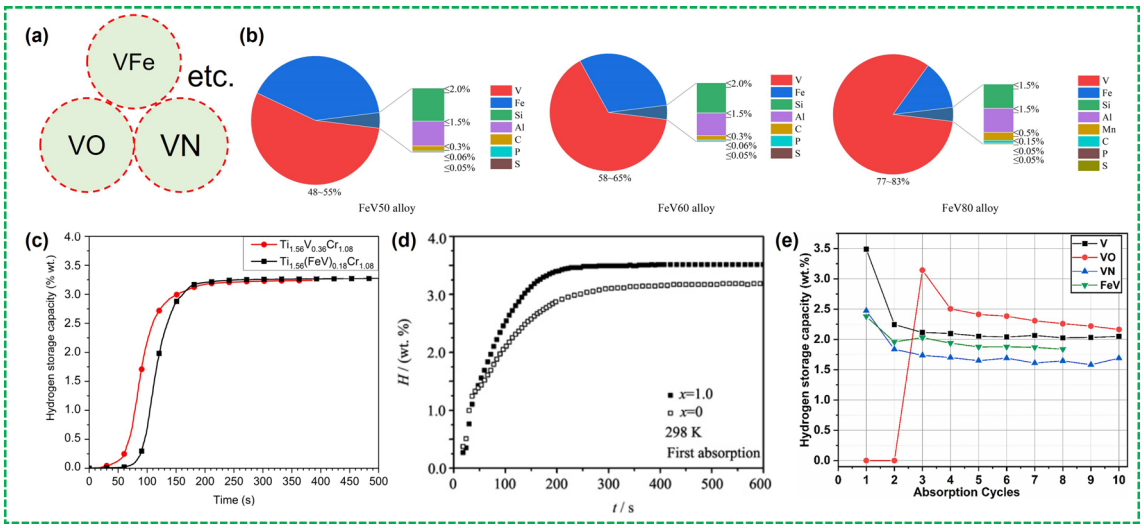

Fig. 9 **a** Diagram of different types of vanadium alloys. **b** Pie chart of chemical composition of different ferrovanadium alloys (FeV50 alloy, FeV60 alloy, and FeV80 alloy in international standard ISO 5451:2022). **c** Activation kinetics of the co-melt $Ti_{1.56}V_{0.18}(FeV)_{0.18}Cr_{1.08}+4\%Zr_7Ni_{10}$ and $Ti_{1.56}V_{0.36}Cr_{1.08}+4\%Zr_7Ni_{10}$ under 20 bars of H_2 at 25 °C. Reproduced with permission from Ref. [182]. **d** First hydrogen absorption kinetics curves measured at 298 K for $Ti_{27.25}Cr_{28.05}V_{37.25}Fe_{7.45}Ce_x$ ($x=0$ and 1.0 at%) alloys. Reproduced with permission from Ref. [75]. Copyright 2010 Elsevier **e** Changes in the hydrogen storage capacity of all alloys with increasing cycles. Reproduced with permission from Ref. [184]. Copyright 2012 Elsevier

activation property due to the appearance of the secondary Laves phase, the hydrogen absorption and desorption capacities were found to have been decreased while the plateau slope factor and pressure were increased [77]. Earlier, we also mentioned that the right amount of silicon could improve the ability to resist poisoning [173]. It is undeniable that the loss of reversible hydrogen storage capacity is inevitable. Huang et al. [103] reported similar results that Si element gave rise to the precipitation of a C14 $TiFe_2$-type Laves phase, resulting in the inhomogeneity of the chemical composition for the $Ti_{26.5}V_{0.45}Fe_{8.5}Cr_{20}Ce_{0.5}$ alloy. Ce could eliminate the negative effects brought by Si, but the mechanism involved is still unclear [183]. The increase of B content will also lead to a decrease of the hydrogen storage capacity of the alloy [61]. Therefore, it is necessary to remove impurities from raw materials.

Several years ago, Chen et al. [73] successfully prepared a $V_{30}Ti_{32}Cr_{32}Fe_6$ alloy from FeV80 alloy that could release 2.35 and 2.56 wt% hydrogen at 298 and 373 K, respectively. Recently, Sharma and Bishnoi compared the hydrogen storage properties of V-base solid solution alloys prepared with different vanadium raw materials (pure V, FeV, VN, and VO). As shown in Fig. 9e, the first hydrogenation process of the 52Ti–12VO–36Cr + 4 wt%Zr alloy prepared by VO alloy did not absorb hydrogen, which was significantly different from the alloy prepared using pure V with no apparent incubation period [184]. This was because that the VO alloy contained 3.4% oxygen, which led to the formation of an oxide layer on the surface of the alloy after melting that impeded the hydrogenation process. However, after two activations, the 52Ti–12VO–36Cr + 4 wt%Zr alloy prepared by VO showed a high hydrogen storage capacity, which was comparable to that of alloy prepared by pureV. This implies the possibility of using low-cost vanadium raw materials to prepare high-performance V–Ti-based solid solution alloys. As we mentioned before, most of the impurity elements in raw materials can be effectively removed by adding metal Ce. On this base, under the premise of using FeV master alloy for achieving large-scale application, it is imperative to improve the output of a single furnace and reduce the composition difference of different batches while ensure the quality stability of V–Ti-based solid solution alloys.

4 Conclusion and Outlook

V–Ti-based solid solution alloys are promising candidates for solid-state metal hydride tanks, which operate under non-extreme temperatures and pressures and supply hydrogen to fuel cells. These alloys, primarily consisting of a body-centered cubic main phase, have attracted much attention due to their high hydrogen storage density at room temperature and adjustable plateau pressure. To explore the application of V–Ti-based solid solution alloys in the field of hydrogen storage, extensive efforts have been initiated, including the optimization of preparing technologies, compositional adjustments, heat treatments, quenching techniques, impurity analysis, and understanding of degradation mechanism. So far, arc melting is still the preferred method for preparing V–Ti solid solution alloys, and V–Ti–Cr and V–Ti–Fe alloys are the two most studied systems. On this basis, the hydrogen storage properties of V–Ti-based solid solution alloys can be improved by adjusting the proportions of V, Ti, Nb, Fe, Ni, Zr, Ce, and other elements. Heat treatment can flatten the plateau and increase reversible hydrogen storage capacity. Although various alloys with excellent hydrogen storage properties have been developed, a reversible hydrogen storage capacity of 2.5 wt% and above seems to be relatively difficult at near-room temperature. And the efficient and stable preparation of V–Ti-based solid solution alloys on large-scale is also a challenge besides the problem of high cost.

To date, many studies only focus on the influence of elements on one aspect of hydrogen storage performance (e.g., activation property) for V–Ti-based solid solution alloys. For practical applications, a modified strategy should be able to address the performance of one aspect while maintaining the performance of other aspects. There are many balances to be considered, such as "ease in activation" vs "high reversible hydrogen storage capacity," "anti-poisoning" and "cost" vs "hydrogen storage capacity."

High vanadium content alloys are currently considered the best option for achieving high reversible hydrogen storage capacity and excellent cyclic stability. The viable method involves the using of a FeV master alloy instead of metallic vanadium, although the impurity removal process still requires further enhancement. Therefore, developing V–Ti-based solid solution alloys that are cost-effective with high

 https://doi.org/10.1007/s40820-025-01672-w

reversible capacities requires relentless effort, particularly for the application of solid-state MH tanks.

Acknowledgements This work was supported by the Key-Area Research and Development Program of Guangdong Province (No.2023B0909060001) and the National Natural Science Foundation of China (No.52271213)

Authors' Contributions Shaoyang Shen contributed to investigation, writing-original draft, writing-review & editing, visualization. Yongan Li contributed to investigation, writing-original draft, writing-review & editing. Liuzhang Ouyang contributed to writing-review & editing, supervision, funding acquisition. Lan Zhang contributed to writing-review & editing. Min Zhu contributed to writing-review & editing. Zongwen Liu contributed to conceptualization, writing-review & editing, supervision.

Declarations

Conflict of Interest The authors declare no interest conflict. They have no known competing financial interests or personal relationships that could have appeared to influence the work reported in this paper. Prof. Zongwen Liu is an editorial board member for Nano-Micro Letters and was not involved in the handling of the review process of this article. All authors declare that there are no competing interests.

References

1. X.L. Zhang, Y.F. Liu, X. Zhang, J.J. Hu, M.X. Gao et al., Empowering hydrogen storage performance of MgH_2 by nanoengineering and nanocatalysis. Mater. Today Nano **9**, 100064 (2020). https://doi.org/10.1016/j.mtnano.2019.100064
2. L. Ouyang, K. Chen, J. Jiang, X.-S. Yang, M. Zhu, Hydrogen storage in light-metal based systems: a review. J. Alloys Compd. **829**, 154597 (2020). https://doi.org/10.1016/j.jallcom.2020.154597
3. M. Hirscher, V.A. Yartys, M. Baricco, J. Bellosta von Colbe, D. Blanchard et al., Materials for hydrogen-based energy storage–past, recent progress and future outlook. J. Alloys Compd. **827**, 153548 (2020). https://doi.org/10.1016/j.jallcom.2019.153548
4. J. Andersson, S. Grönkvist, Large-scale storage of hydrogen. Int. J. Hydrog. Energy **44**, 11901–11919 (2019). https://doi.org/10.1016/j.ijhydene.2019.03.063
5. E. Rivard, M. Trudeau, K. Zaghib, Hydrogen storage for mobility: a review. Materials **12**, 1973 (2019). https://doi.org/10.3390/ma12121973
6. Z. Peng, Q. Li, L. Ouyang, W. Jiang, K. Chen et al., Overview of hydrogen compression materials based on a three-stage metal hydride hydrogen compressor. J. Alloys Compd. **895**, 162465 (2022). https://doi.org/10.1016/j.jallcom.2021.162465
7. W. Jiang, C. He, X. Yang, X. Xiao, L. Ouyang et al., Influence of element substitution on structural stability and hydrogen storage performance: a theoretical and experimental study on $TiCr_{2-x}Mn_x$ alloy. Renew. Energy **197**, 564–573 (2022). https://doi.org/10.1016/j.renene.2022.07.113
8. L. Ren, Y. Li, Z. Li, X. Lin, C. Lu et al., Boosting hydrogen storage performance of MgH_2 by oxygen vacancy-rich H-V_2O_5 nanosheet as an excited H-pump. Nano-Micro Lett. **16**, 160 (2024). https://doi.org/10.1007/s40820-024-01375-8
9. L. Ren, W. Zhu, Y. Li, X. Lin, H. Xu et al., Oxygen vacancy-rich 2D TiO_2 nanosheets: a bridge toward high stability and rapid hydrogen storage kinetics of nano-confined MgH_2. Nano-Micro Lett. **14**, 144 (2022). https://doi.org/10.1007/s40820-022-00891-9
10. Y. Shang, C. Pistidda, G. Gizer, T. Klassen, M. Dornheim, Mg-based materials for hydrogen storage. J. Magnes. Alloys **9**, 1837–1860 (2021). https://doi.org/10.1016/j.jma.2021.06.007
11. Q. Li, Y. Lu, Q. Luo, X. Yang, Y. Yang et al., Thermodynamics and kinetics of hydriding and dehydriding reactions in Mg-based hydrogen storage materials. J. Magnes. Alloys **9**, 1922–1941 (2021). https://doi.org/10.1016/j.jma.2021.10.002
12. H. Hu, C. Ma, Q. Chen, Mechanism and microstructural evolution of TiCrVFe hydrogen storage alloys upon de-/ hydrogenation. J. Alloys Compd. **877**, 160315 (2021). https://doi.org/10.1016/j.jallcom.2021.160315
13. L. Ren, Y. Li, N. Zhang, Z. Li, X. Lin et al., Nanostructuring of Mg-based hydrogen storage materials: recent advances for promoting key applications. Nano-Micro Lett. **15**, 93 (2023). https://doi.org/10.1007/s40820-023-01041-5
14. L. Ouyang, F. Liu, H. Wang, J. Liu, X.-S. Yang et al., Magnesium-based hydrogen storage compounds: a review. J. Alloys Compd. **832**, 154865 (2020). https://doi.org/10.1016/j.jallcom.2020.154865
15. L. Ouyang, Z. Cao, H. Wang, R. Hu, M. Zhu, Application of dielectric barrier discharge plasma-assisted milling in energy storage materials—a review. J. Alloys Compd. **691**, 422–435 (2017). https://doi.org/10.1016/j.jallcom.2016.08.179
16. S. Shen, W. Liao, Z. Cao, J. Liu, H. Wang et al., Enhanced hydrogen storage properties of MgH_2 with the co-addition of $LiBH_4$ and YNi_5 alloy. J. Mater. Sci. Technol. **178**, 90–99 (2024). https://doi.org/10.1016/j.jmst.2023.08.039

17. S. Shen, L. Ouyang, J. Liu, H. Wang, X.-S. Yang et al., In situ formed ultrafine metallic Ni from nickel (II) acetylacetonate precursor to realize an exceptional hydrogen storage performance of MgH_2-Ni-EG nanocomposite. J. Magnes. Alloys **11**, 3174–3185 (2023). https://doi.org/10.1016/j.jma.2021.12.003
18. W. Liao, W. Jiang, X.-S. Yang, H. Wang, L. Ouyang et al., Enhancing (de)hydrogenation kinetics properties of the Mg/MgH_2 system by adding ANi_5 (A = Ce, Nd, Pr, Sm, and Y) alloys via ball milling. J. Rare Earths **39**, 1010–1016 (2021). https://doi.org/10.1016/j.jre.2020.07.020
19. J. Zhang, H. Li, X. Xiao, L. Ouyang, Preparation and regeneration of metal borohydrides for high-density hydrogen supply: progress, challenges, and perspectives. J. Alloys Compd. **951**, 169887 (2023). https://doi.org/10.1016/j.jallcom.2023.169887
20. Y. Zhu, L. Ouyang, H. Zhong, J. Liu, H. Wang et al., Closing the loop for hydrogen storage: facile regeneration of $NaBH_4$ from its hydrolytic product. Angew. Chem. Int. Ed. **59**, 8623–8629 (2020). https://doi.org/10.1002/anie.201915988
21. K. Chen, L. Ouyang, H. Zhong, J. Liu, H. Wang et al., Converting H^+ from coordinated water into H^- enables super facile synthesis of $LiBH_4$. Green Chem. **21**, 4380–4387 (2019). https://doi.org/10.1039/c9gc01897b
22. L. Ouyang, W. Chen, J. Liu, M. Felderhoff, H. Wang et al., Enhancing the regeneration process of consumed $NaBH_4$ for hydrogen storage. Adv. Energy Mater. **7**, 1700299 (2017). https://doi.org/10.1002/aenm.201700299
23. S. Kumar, A. Jain, T. Ichikawa, Y. Kojima, G.K. Dey, Development of vanadium based hydrogen storage material: a review. Renew. Sustain. Energy Rev. **72**, 791–800 (2017). https://doi.org/10.1016/j.rser.2017.01.063
24. H. Itoh, H. Arashima, K. Kubo, T. Kabutomori, K. Ohnishi, Improvement of cyclic durability of BCC structured Ti–Cr–V alloys. J. Alloys Compd. **404**, 417–420 (2005). https://doi.org/10.1016/j.jallcom.2004.12.175
25. K. Goshome, N. Endo, M. Tetsuhiko, Evaluation of a BCC alloy as metal hydride compressor via 100 MPa-class high-pressure hydrogen apparatus. Int. J. Hydrog. Energy **44**, 10800–10807 (2019). https://doi.org/10.1016/j.ijhydene.2019.03.008
26. M. Balcerzak, Structure and hydrogen storage properties of mechanically alloyed Ti–V alloys. Int. J. Hydrog. Energy **42**, 23698–23707 (2017). https://doi.org/10.1016/j.ijhydene.2017.03.224
27. L. Pickering, D. Reed, A.I. Bevan, D. Book, Ti–V–Mn based metal hydrides for hydrogen compression applications. J. Alloys Compd. **645**, S400–S403 (2015). https://doi.org/10.1016/j.jallcom.2014.12.098
28. H. Miao, W.G. Wang, Mechanisms of improving the cyclic stability of V–Ti-based hydrogen storage electrode alloys. J. Alloys Compd. **508**, 592–598 (2010). https://doi.org/10.1016/j.jallcom.2010.08.132
29. M. Gao, S. Zhang, H. Miao, Y. Liu, H. Pan, Pulverization mechanism of the multiphase Ti–V-based hydrogen storage electrode alloy during charge/discharge cycling. J. Alloys Compd. **489**, 552–557 (2010). https://doi.org/10.1016/j.jallcom.2009.09.107
30. Y. Zhu, H. Pan, M. Gao, Y. Liu, R. Li et al., Degradation mechanisms of Ti–V-based multiphase hydrogen storage alloy electrode. Int. J. Hydrog. Energy **29**, 313–318 (2004). https://doi.org/10.1016/S0360-3199(03)00153-8
31. Q.A. Zhang, Y.Q. Lei, L.X. Chen, Q.D. Wang, Electrochemical behaviors of a $V_3TiNi_{0.56}Hf_{0.24}$ alloy electrode during charge–discharge cycling. Mater. Chem. Phys. **71**, 58–61 (2001). https://doi.org/10.1016/S0254-0584(01)00269-3
32. M.D. Dolan, M.A. Kochanek, C.N. Munnings, K.G. McLennan, D.M. Viano, Hydride phase equilibria in V–Ti–Ni alloy membranes. J. Alloys Compd. **622**, 276–281 (2015). https://doi.org/10.1016/j.jallcom.2014.10.081
33. S. Suwarno, Y. Gosselin, J.K. Solberg, J.P. Maehlen, M. Williams et al., Selective hydrogen absorption from gaseous mixtures by BCC Ti–V alloys. Int. J. Hydrog. Energy **37**, 4127–4138 (2012). https://doi.org/10.1016/j.ijhydene.2011.11.100
34. T.M. Adams, J. Mickalonis, Hydrogen permeability of multiphase V–Ti–Ni metallic membranes. Mater. Lett. **61**, 817–820 (2007). https://doi.org/10.1016/j.matlet.2006.05.078
35. S.-W. Cho, E. Akiba, Y. Nakamura, H. Enoki, Hydrogen isotope effects in $Ti_{1.0}Mn_{0.9}V_{1.1}$ and $Ti_{1.0}Cr_{1.5}V_{1.7}$ alloys. J. Alloys Compd. **297**, 253–260 (2000). https://doi.org/10.1016/S0925-8388(99)00585-X
36. E. Akiba, H. Iba, Hydrogen absorption by Laves phase related BCC solid solution. Intermetallics **6**, 461–470 (1998). https://doi.org/10.1016/S0966-9795(97)00088-5
37. S. Ono, K. Nomura, Y. Ikeda, The reaction of hydrogen with alloys of vanadium and titanium. J. Less Common Met. **72**, 159–165 (1980). https://doi.org/10.1016/0022-5088(80)90135-6
38. Y. Fei, X. Kong, Z. Wu, H. Li, V.K. Peterson, In situ neutron-diffraction study of the $Ti_{38}V_{30}Cr_{14}Mn_{18}$ structure during hydrogenation. J. Power Sources **241**, 355–358 (2013). https://doi.org/10.1016/j.jpowsour.2013.04.118
39. Y. Wu, W. Zhao, L. Jiang, Z. Li, X. Guo et al., Effect of Fe and Al on hydrogen storage properties of 75 V–Ti–Cr alloys. J. Alloys Compd. **887**, 161181 (2021). https://doi.org/10.1016/j.jallcom.2021.161181
40. X.Y. Chen, R.R. Chen, K. Yu, X. Ding, X.Z. Li et al., Effect of Ce substitution on hydrogen absorption/desorption of Laves phase-related BCC solid solution $Ti_{33}V_{37}Mn_{30}$ alloy. J. Alloys Compd. **783**, 617–624 (2019). https://doi.org/10.1016/j.jallcom.2018.12.302
41. P. Ruz, S. Banerjee, R. Halder, A. Kumar, V. Sudarsan, Thermodynamics, kinetics and microstructural evolution of $Ti_{0.43}Zr_{0.07}Cr_{0.25}V_{0.25}$ alloy upon hydrogenation. Int. J. Hydrog. Energy **42**, 11482–11492 (2017). https://doi.org/10.1016/j.ijhydene.2017.02.184
42. J.M. Abdul, L.H. Chown, Influence of Fe on hydrogen storage properties of V-rich ternary alloys. Int. J. Hydrog. Energy **41**, 2781–2787 (2016). https://doi.org/10.1016/j.ijhydene.2015.11.154

 https://doi.org/10.1007/s40820-025-01672-w

43. S.-I. Towata, T. Noritake, A. Itoh, M. Aoki, K. Miwa, Effect of partial niobium and iron substitution on short-term cycle durability of hydrogen storage Ti–Cr–V alloys. Int. J. Hydrog. Energy **38**, 3024–3029 (2013). https://doi.org/10.1016/j.ijhydene.2012.12.100
44. Z. Dehouche, M. Savard, F. Laurencelle, J. Goyette, Ti–V–Mn based alloys for hydrogen compression system. J. Alloys Compd. **400**, 276–280 (2005). https://doi.org/10.1016/j.jallcom.2005.04.007
45. C. Raufast, D. Planté, S. Miraglia, Investigation of the structural and hydrogenation properties of disordered Ti–V–Cr-Mo BCC solid solutions. J. Alloys Compd. **617**, 633–638 (2014). https://doi.org/10.1016/j.jallcom.2014.07.089
46. Z. Hang, X. Xiao, K. Yu, S. Li, C. Chen et al., Influence of Fe content on the microstructure and hydrogen storage properties of $Ti_{16}Zr_5Cr_{22}V_{57-x}Fe_x$ (x =2–8) alloys. Int. J. Hydrog. Energy **35**, 8143–8148 (2010). https://doi.org/10.1016/j.ijhydene.2009.12.184
47. X.B. Yu, Z. Wu, B.J. Xia, N.X. Xu, The activation mechanism of Ti–V-based hydrogen storage alloys. J. Alloys Compd. **375**, 221–223 (2004). https://doi.org/10.1016/j.jallcom.2003.11.027
48. M. Taghizadeh, S.M. Abbasi, M. Seifollahi, S.M.G. Mirsaeed, The effect of remelting on microstructure and hydrogen storage properties of Ti–Mn–V alloy. Trans. Indian Inst. Met. **74**, 811–816 (2021). https://doi.org/10.1007/s12666-020-02178-2
49. Z. Chen, L. Luo, Z. Su, W. Liu, F. Zhang et al., Effect of LaH_3 additive on microstructures and hydrogen storage properties of $V_{40}Ti_{26}Cr_{26}Fe_8$ alloys prepared by hydride powder sintering method. Int. J. Hydrog. Energy **44**, 13538–13548 (2019). https://doi.org/10.1016/j.ijhydene.2019.03.038
50. Y. Mao, S. Yang, C. Wu, L. Luo, Y. Chen, Preparation of $(FeV80)_{48}Ti_{26+x}Cr_{26}$($x$=0–4) alloys by the hydride sintering method and their hydrogen storage performance. J. Alloys Compd. **705**, 533–538 (2017). https://doi.org/10.1016/j.jallcom.2017.02.166
51. S. Kumar, P.K. Singh, Y. Kojima, V. Kain, Cyclic hydrogen storage properties of VTiCrAl alloy. Int. J. Hydrog. Energy **43**, 7096–7101 (2018). https://doi.org/10.1016/j.ijhydene.2018.02.103
52. A. Kawabata, H. Yoshinaga, M. Tsukahara, T. Sakai, S. Sakurai et al., A novel thermic process for producing V-based solid solution type hydrogen storage alloy. Mater. Trans. **42**, 1794–1799 (2001). https://doi.org/10.2320/matertrans.42.1794
53. M. Balcerzak, Structural, electrochemical and hydrogen sorption studies of nanocrystalline Ti–V-Co and Ti–V–Ni-Co alloys synthesized by mechanical alloying method. J. Mater. Eng. Perform. **28**, 4838–4844 (2019). https://doi.org/10.1007/s11665-019-04266-x
54. A. Dagher, H.G. Salem, T.M. Moustafa, E.B. Mettawee, E. Abdel-Rahman, Hydrogen absorption characteristics of mechanically alloyed Ti–Zr–Ni and Ti–V–Ni powders. Int. J. Hydrog. Energy **39**, 17740–17746 (2014). https://doi.org/10.1016/j.ijhydene.2014.08.109
55. J.-Y. Wang, Comparison of hydrogen storage properties of $Ti_{0.37}V_{0.38}Mn_{0.25}$ alloys prepared by mechanical alloying and vacuum arc melting. Int. J. Hydrog. Energy **34**, 3771–3777 (2009). https://doi.org/10.1016/j.ijhydene.2009.02.028
56. S. Couillaud, H. Enoki, S. Amira, J.L. Bobet, E. Akiba et al., Effect of ball milling and cold rolling on hydrogen storage properties of nanocrystalline $TiV_{1.6}Mn_{0.4}$ alloy. J. Alloys Compd. **484**, 154–158 (2009). https://doi.org/10.1016/j.jallcom.2009.05.037
57. J. Huot, H. Enoki, E. Akiba, Synthesis, phase transformation, and hydrogen storage properties of ball-milled $TiV_{0.9}Mn_{1.1}$. J. Alloys Compd. **453**, 203–209 (2008). https://doi.org/10.1016/j.jallcom.2006.11.193
58. B.K. Singh, G. Shim, S.-W. Cho, Effects of mechanical milling on hydrogen storage properties of $Ti_{0.32}$ $Cr_{0.43}V_{0.25}$ alloy. Int. J. Hydrog. Energy **32**, 4961–4965 (2007). https://doi.org/10.1016/j.ijhydene.2007.07.010
59. D. Cauceglia, M.D. Hampton, J.K. Lomness, D.K. Slattery, M. Resan, Hydrogen uptake characteristics of mechanically alloyed TiVNi. J. Alloys Compd. **417**, 159–163 (2006). https://doi.org/10.1016/j.jallcom.2005.01.143
60. H.-B. Wang, Q. Wang, C. Dong, F. Xu, L.-X. Sun et al., Microstructure and storage properties of low V-containing Ti–Cr–V hydrogen storage alloys prepared by arc melting and suction casting. Rare Met. **32**, 354–358 (2013). https://doi.org/10.1007/s12598-013-0101-6
61. M. Uno, K. Takahashi, T. Maruyama, H. Muta, S. Yamanaka, Hydrogen solubility of BCC titanium alloys. J. Alloys Compd. **366**, 213–216 (2004). https://doi.org/10.1016/S0925-8388(03)00749-7
62. H. Arashima, F. Takahashi, T. Ebisawa, H. Itoh, T. Kabutomori, Correlation between hydrogen absorption properties and homogeneity of Ti–Cr–V alloys. J. Alloys Compd. **356**, 405–408 (2003). https://doi.org/10.1016/S0925-8388(03)00363-3
63. S. Suwarno, J.K. Solberg, J.P. Maehlen, B. Krogh, B.T. Børresen et al., Microstructure and hydrogen storage properties of as-cast and rapidly solidified Ti-rich Ti–V alloys. Trans. Nonferrous Met. Soc. China **22**, 1831–1838 (2012). https://doi.org/10.1016/s1003-6326(11)61394-0
64. I. Kunce, M. Polanski, J. Bystrzycki, Microstructure and hydrogen storage properties of a TiZrNbMoV high entropy alloy synthesized using Laser Engineered Net Shaping (LENS). Int. J. Hydrog. Energy **39**, 9904–9910 (2014). https://doi.org/10.1016/j.ijhydene.2014.02.067
65. B.K. Singh, S.W. Cho, K.S. Bartwal, Microstructure and hydrogen storage properties of $(Ti_{0.32}Cr_{0.43}V_{0.25})$ + x wt% La (x = 0–10) alloys. Int. J. Hydrog. Energy **39**, 8351–8356 (2014). https://doi.org/10.1016/j.ijhydene.2014.03.168
66. M. Aoki, T. Noritake, A. Ito, M. Ishikiriyama, S.-I. Towata, Improvement of cyclic durability of Ti–Cr–V alloy by Fe substitution. Int. J. Hydrog. Energy **36**, 12329–12332 (2011). https://doi.org/10.1016/j.ijhydene.2011.07.019

67. J.-H. Yoo, G. Shim, C.-N. Park, W.-B. Kim, S.-W. Cho, Influence of Mn or Mn plus Fe on the hydrogen storage properties of the Ti–Cr–V alloy. Int. J. Hydrog. Energy **34**, 9116–9121 (2009). https://doi.org/10.1016/j.ijhydene.2009.08.064
68. J. Chen, Z. Li, H. Huang, Y. Lv, B. Liu et al., Superior cycle life of TiZrFeMnCrV high entropy alloy for hydrogen storage. Scr. Mater. **212**, 114548 (2022). https://doi.org/10.1016/j.scriptamat.2022.114548
69. V. Zadorozhnyy, I. Tomilin, E. Berdonosova, C. Gammer, M. Zadorozhnyy et al., Composition design, synthesis and hydrogen storage ability of multi-principAl–component alloy TiVZrNbTa. J. Alloys Compd. **901**, 163638 (2022). https://doi.org/10.1016/j.jallcom.2022.163638
70. T. Kuriiwa, T. Maruyama, A. Kamegawa, M. Okada, Effects of V content on hydrogen storage properties of V–Ti–Cr alloys with high desorption pressure. Int. J. Hydrog. Energy **35**, 9082–9087 (2010). https://doi.org/10.1016/j.ijhydene.2010.06.024
71. D.P. Sai, N. Kumar, V. Saxena, Analysis of the potential metal hydrides for hydrogen storage in automobile applications, in *Advanced Combustion for Sustainable Transport* (Springer Singapore, 2021), pp. 299–330. https://doi.org/10.1007/978-981-16-8418-0_10
72. S.F. Santos, J. Huot, Hydrogen storage in $TiCr_{1.2}(FeV)_x$ BCC solid solutions. J. Alloys Compd. **472**, 247–251 (2009). https://doi.org/10.1016/j.jallcom.2008.04.062
73. Y. Yan, Y. Chen, C. Wu, M. Tao, H. Liang, A low-cost BCC alloy prepared from a FeV80 alloy with a high hydrogen storage capacity. J Power Sources **164**, 799–802 (2007). https://doi.org/10.1016/j.jpowsour.2006.10.097
74. Z. Hang, X. Xiao, S. Li, H. Ge, C. Chen et al., Influence of heat treatment on the microstructure and hydrogen storage properties of $Ti_{10}V_{77}Cr_6Fe_6Zr$ alloy. J. Alloys Compd. **529**, 128–133 (2012). https://doi.org/10.1016/j.jallcom.2012.03.044
75. J. Mi, F. Lü, X. Liu, L. Jiang, Z. Li et al., Enhancement of cerium and hydrogen storage property of a low-cost Ti–V based BCC alloy prepared by commercial ferrovanadium. J. Rare Earths **28**, 781–784 (2010). https://doi.org/10.1016/S1002-0721(09)60200-3
76. X. Liu, L. Jiang, Z. Li, Z. Huang, S. Wang, Improve plateau property of $Ti_{32}Cr_{46}V_{22}$ BCC alloy with heat treatment and Ce additive. J. Alloys Compd. **471**, L36–L38 (2009). https://doi.org/10.1016/j.jallcom.2008.04.004
77. Y. Yan, Y. Chen, H. Liang, C. Wu, M. Tao, The effect of Si on $V_{30}Ti_{35}Cr_{25}Fe_{10}$ BCC hydrogen storage alloy. J. Alloys Compd. **441**, 297–300 (2007). https://doi.org/10.1016/j.jallcom.2006.09.096
78. C. Wu, X. Zheng, Y. Chen, M. Tao, G. Tong et al., Hydrogen storage and cyclic properties of $V_{60}Ti_{(21.4+x)}Cr_{(66-x)}Fe_{12}$ ($0 \le x \le 3$) alloys. Int. J. Hydrog. Energy **35**, 8130–8135 (2010). https://doi.org/10.1016/j.ijhydene.2010.01.017
79. X.B. Yu, Z. Wu, B.J. Xia, N.X. Xu, Hydrogen storage performance of quenched Ti–V-based alloy. J. Alloys Compd. **373**, 134–136 (2004). https://doi.org/10.1016/j.jallcom.2003.10.030
80. S.-I. Towata, T. Noritake, A. Itoh, M. Aoki, K. Miwa, Cycle durability of Ti–Cr–V alloys partially substituted by Nb or Fe. J. Alloys Compd. **580**, S226–S228 (2013). https://doi.org/10.1016/j.jallcom.2013.03.163
81. X.B. Yu, J.Z. Chen, Z. Wu, B.J. Xia, N.X. Xu, Effect of Cr content on hydrogen storage properties for Ti–V-based BCC-phase alloys. Int. J. Hydrog. Energy **29**, 1377–1381 (2004). https://doi.org/10.1016/j.ijhydene.2004.01.015
82. X.B. Yu, Z.X. Yang, S.L. Feng, Z. Wu, N.X. Xu, Influence of Fe addition on hydrogen storage characteristics of Ti–V-based alloy. Int. J. Hydrog. Energy **31**, 1176–1181 (2006). https://doi.org/10.1016/j.ijhydene.2005.09.008
83. M. Tsukahara, Hydrogenation properties of vanadium-based alloys with large hydrogen storage capacity. Mater. Trans. **52**, 68–72 (2011). https://doi.org/10.2320/matertrans.m2010216
84. T. Matsunaga, M. Kon, K. Washio, T. Shinozawa, M. Ishikiriyama, TiCrVMo alloys with high dissociation pressure for high-pressure MH tank. Int. J. Hydrog. Energy **34**, 1458–1462 (2009). https://doi.org/10.1016/j.ijhydene.2008.11.061
85. R.R. Chen, X.Y. Chen, X. Ding, X.Z. Li, J.J. Guo et al., Effects of Ti/Mn ratio on microstructure and hydrogen storage properties of Ti–V–Mn alloys. J. Alloys Compd. **748**, 171–178 (2018). https://doi.org/10.1016/j.jallcom.2018.03.154
86. M. Shibuya, J. Nakamura, H. Enoki, E. Akiba, High-pressure hydrogenation properties of Ti–V–Mn alloy for hybrid hydrogen storage vessel. J. Alloys Compd. **475**, 543–545 (2009). https://doi.org/10.1016/j.jallcom.2008.07.121
87. H. Hu, C. Ma, Q. Chen, Improved hydrogen storage properties of Ti_2CrV alloy by Mo substitutional doping. Int. J. Hydrog. Energy **47**, 11929–11937 (2022). https://doi.org/10.1016/j.ijhydene.2022.01.212
88. C.-Y. Seo, Z.-L. Zhang, J.-H. Kim, P.S. Lee, J.-Y. Lee, Effect of manganese addition on hydrogen storage performance of vanadium-based BCC hydrogen storage alloys. Met. Mater. Int. **8**, 341–346 (2002). https://doi.org/10.1007/BF03186105
89. X.P. Liu, F. Cuevas, L.J. Jiang, M. Latroche, Z.N. Li et al., Improvement of the hydrogen storage properties of Ti–Cr–V–Fe BCC alloy by Ce addition. J. Alloys Compd. **476**, 403–407 (2009). https://doi.org/10.1016/j.jallcom.2008.09.042
90. X.Y. Chen, R.R. Chen, X. Ding, H.Z. Fang, J.J. Guo et al., Crystal structure and hydrogen storage properties of Ti–V–Mn alloys. Int. J. Hydrog. Energy **43**, 6210–6218 (2018). https://doi.org/10.1016/j.ijhydene.2018.02.009
91. X.Y. Chen, R.R. Chen, X. Ding, S. Wang, Y.Q. Su et al., Activation and de/hydriding behavior in $Ti_{23}V_{40}Mn_{37}$ alloy by Hf and Hf/Cr substitutions. Int. J. Hydrog. Energy **45**, 6813–6822 (2020). https://doi.org/10.1016/j.ijhydene.2019.12.194
92. X.Y. Chen, R.R. Chen, X. Ding, X.Z. Li, H.S. Ding et al., Substitution effect of Hf on hydrogen storage capacity and cycling durability of $Ti_{23}V_{40}Mn_{37}$ metal hydride alloys. Int. J. Hydrog. Energy **43**, 19567–19574 (2018). https://doi.org/10.1016/j.ijhydene.2018.08.203
93. L. Luo, Y. Li, T. Zhai, F. Hu, Z. Zhao et al., Microstructure and hydrogen storage properties of $V_{48}Fe_{12}Ti_{15-x}Cr_{25}Al_x$

 https://doi.org/10.1007/s40820-025-01672-w

(x=0, 1) alloys. Int. J. Hydrog. Energy **44**, 25188–25198 (2019). https://doi.org/10.1016/j.ijhydene.2019.02.172

94. J. Mi, X. Liu, Y. Li, L. Jiang, Z. Li et al., Effect of cerium content on microstructure and hydrogen storage performance of $Ti_{24}Cr_{17.5}V_{50}Fe_{85}Ce_x$ (x=0–1.0) alloys. J. Rare Earths **27**, 154–158 (2009). https://doi.org/10.1016/S1002-0721(08)60211-2
95. B.K. Singh, S.-W. Cho, K.S. Bartwal, Effect on structure and hydrogen storage characteristics of composite alloys $Ti_{0.32}Cr_{0.43}V_{0.25}$ with $LaNi_5$ and rare-earth elements La, Ce, Y. J. Alloys Compd. **478**, 785–788 (2009). https://doi.org/10.1016/j.jallcom.2008.12.011
96. C.L. Wu, Y.G. Yan, Y.G. Chen, M.D. Tao, X. Zheng, Effect of rare earth (RE) elements on V-based hydrogen storage alloys. Int. J. Hydrog. Energy **33**, 93–97 (2008). https://doi.org/10.1016/j.ijhydene.2007.09.002
97. Y. Yan, Y. Chen, H. Liang, X. Zhou, C. Wu et al., Effect of Ce on the structure and hydrogen storage properties of $V_{55}Ti_{22.5}Cr_{16.1}Fe_{6.4}$. J. Alloys Compd. **429**, 301–305 (2007). https://doi.org/10.1016/j.jallcom.2006.04.057
98. K. Shashikala, S. Banerjee, A. Kumar, M.R. Pai, C.G.S. Pillai, Improvement of hydrogen storage properties of TiCrV alloy by Zr substitution for Ti. Int. J. Hydrog. Energy **34**, 6684–6689 (2009). https://doi.org/10.1016/j.ijhydene.2009.06.065
99. S. Basak, K. Shashikala, S.K. Kulshreshtha, Hydrogen absorption characteristics of Zr substituted $Ti_{0.85}VFe_{0.15}$ alloy. Int. J. Hydrog. Energy **33**, 350–355 (2008). https://doi.org/10.1016/j.ijhydene.2007.07.023
100. A. Kamble, P. Sharma, J. Huot, Effect of addition of Zr, Ni, and Zr-Ni alloy on the hydrogen absorption of Body Centred Cubic 52Ti–12V–36Cr alloy. Int. J. Hydrog. Energy **43**, 7424–7429 (2018). https://doi.org/10.1016/j.ijhydene.2018.02.106
101. J.-H. Yoo, G. Shim, S.-W. Cho, C.-N. Park, Effects of desorption temperature and substitution of Fe for Cr on the hydrogen storage properties of $Ti_{0.32}Cr_{0.43}V_{0.25}$ alloy. Int. J. Hydrog. Energy **32**, 2977–2981 (2007). https://doi.org/10.1016/j.ijhydene.2007.01.012
102. T. Mouri, H. Iba, Hydrogen-absorbing alloys with a large capacity for a new energy carrier. Mater. Sci. Eng. A **329**, 346–350 (2002). https://doi.org/10.1016/S0921-5093(01)01597-0
103. Z. Huang, F. Cuevas, X. Liu, L. Jiang, S. Wang et al., Effects of Si addition on the microstructure and the hydrogen storage properties of $Ti_{2.65}V_{45}Fe_{8.5}Cr_{20}Ce_{0.5}$ BCC solid solution alloys. Int. J. Hydrog. Energy **34**, 9385–9392 (2009). https://doi.org/10.1016/j.ijhydene.2009.09.055
104. J. Mi, X. Guo, X. Liu, L. Jiang, Z. Li et al., Effect of Al on microstructures and hydrogen storage properties of $Ti_{2.65}Cr_{20}(V_{0.45}Fe_{0.085})_{100-x}Al_xCe_{0.5}$ alloy. J. Alloys Compd. **485**, 324–327 (2009). https://doi.org/10.1016/j.jallcom.2009.05.096
105. Y. Yan, Y. Chen, H. Liang, C. Wu, M. Tao et al., Effect of Al on hydrogen storage properties of $V_{30}Ti_{35}Cr_{25}Fe_{10}$ alloy. J. Alloys Compd. **426**, 253–255 (2006). https://doi.org/10.1016/j.jallcom.2005.12.122
106. J.-H. Yoo, G. Shim, J.-S. Yoon, S.-W. Cho, Effects of substituting Al for Cr in the $Ti_{0.32}Cr_{0.43}V_{0.25}$ alloy on its microstructure and hydrogen storage properties. Int. J. Hydrog. Energy **34**, 1463–1467 (2009). https://doi.org/10.1016/j.ijhydene.2008.11.102
107. U. Ulmer, K. Asano, T. Bergfeldt, V.S.K. Chakravadhanula, R. Dittmeyer et al., Effect of oxygen on the microstructure and hydrogen storage properties of V–Ti–Cr–Fe quaternary solid solutions. Int. J. Hydrog. Energy **39**, 20000–20008 (2014). https://doi.org/10.1016/j.ijhydene.2014.08.152
108. S. Selvaraj, A. Jain, S. Kumar, T. Zhang, S. Isobe et al., Study of cyclic performance of V–Ti–Cr alloys employed for hydrogen compressor. Int. J. Hydrog. Energy **43**, 2881–2889 (2018). https://doi.org/10.1016/j.ijhydene.2017.12.159
109. A. Martínez, D.S. dos Santos, Influence of the substitution of V by Nb in the structure and properties of hydrogen absorption/desorption of $TiCr_{1.1}V_{0.9}$ alloy. J. Alloys Compd. **536**, S231–S235 (2012). https://doi.org/10.1016/j.jallcom.2011.11.092
110. B.H. Silva, C. Zlotea, G. Vaughan, Y. Champion, W.J. Botta et al., Hydrogen absorption/desorption reactions of the $(TiVNb)_{85}Cr_{15}$ multicomponent alloy. J. Alloys Compd. **901**, 163620 (2022). https://doi.org/10.1016/j.jallcom.2022.163620
111. S. Yang, F. Yang, C. Wu, Y. Chen, Y. Mao et al., Hydrogen storage and cyclic properties of $(VFe)_{60}(TiCrCo)_{40-x}Zr_x$ ($0 \le x \le 2$) alloys. J. Alloys Compd. **663**, 460–465 (2016). https://doi.org/10.1016/j.jallcom.2015.12.125
112. T. Kuriiwa, T. Tamura, T. Amemiya, T. Fuda, A. Kamegawa et al., New V-based alloys with high Protium absorption and desorption capacity. J. Alloys Compd. **293**, 433–436 (1999). https://doi.org/10.1016/S0925-8388(99)00325-4
113. Q. Zeng, F. Wang, Z. Li, M. Rong, J. Wang et al., Influence of Zr addition on the microstructure and hydrogenation kinetics of $Ti_{50-x}V_{25}Cr_{25}Zr_x$ (x = 0, 5, 7, and 9) alloys. Materials **17**, 1366 (2024). https://doi.org/10.3390/ma17061366
114. S. Zhang, X. Ding, R. Chen, J. Zhang, Y. Su et al., Modification of nano-eutectic structure and the relation on hydrogen storage properties: a novel Ti–V–Zr medium entropy alloy. Int. J. Hydrog. Energy **47**, 34533–34544 (2022). https://doi.org/10.1016/j.ijhydene.2022.08.039
115. B. Liu, X. Chen, L. Shang, Q. Tao, R. Chen, Crucial role of Zr_xNi_y addition during hydrogen absorption/desorption of $Ti_{37}V_{40}Mn_{23}$ alloy. J. Alloys Compd. **997**, 174840 (2024). https://doi.org/10.1016/j.jallcom.2024.174840
116. A. Kamble, P. Sharma, J. Huot, Effect of the addition of 4 wt% Zr to BCC solid solution $Ti_{52}V_{12}Cr_{36}$ at melting/milling on hydrogen sorption properties. Front. Mater. **8**, 821126 (2022). https://doi.org/10.3389/fmats.2021.821126
117. H. Kwon, J. Kim, S.-W. Cho, J.-H. Yoo, K.-M. Roh et al., The effect of Sc addition on the hydrogen storage capacity of $Ti_{0.32}Cr_{0.43}V_{0.25}$ alloy. Int. J. Hydrog. Energy **39**, 10600–10605 (2014). https://doi.org/10.1016/j.ijhydene.2014.05.011

118. J. Zhu, L. Ma, F. Liang, L. Wang, Effect of Sc substitution on hydrogen storage properties of Ti–V–Cr–Mn alloys. Int. J. Hydrog. Energy **40**, 6860–6865 (2015). https://doi.org/10.1016/j.ijhydene.2015.03.149
119. L. Luo, H. Han, D. Feng, W. Lv, L. Chen et al., Nanocrystalline high entropy alloys with ultrafast kinetics and high storage capacity for large-scale room-temperature-applicable hydrogen storage. Renewables **2**, 138–149 (2024). https://doi.org/10.31635/renewables.024.202300049
120. X. Zhang, H. Xiao, X. He, R. Tang, W. Zhou et al., Impacts of Y dopants on the microstructure and cyclic stability of TiCrVFeMo alloys. Int. J. Hydrog. Energy **61**, 1220–1229 (2024). https://doi.org/10.1016/j.ijhydene.2024.02.330
121. F. Liang, N. Ding, W. Liu, H. Yan, L. Wang, Superior reversible hydrogen storage capacity of V-based solid solution alloy above atmospheric pressure with yttrium substitution. Mater. Lett. **297**, 129945 (2021). https://doi.org/10.1016/j.matlet.2021.129945
122. M. de Brito Ferraz, W.J. Botta, G. Zepon, Synthesis, characterization and first hydrogen absorption/desorption of the $Mg_{35}Al_{15}Ti_{25}V_{10}Zn_{15}$ high entropy alloy. Int. J. Hydrog. Energy **47**, 22881–22892 (2022). https://doi.org/10.1016/j.ijhydene.2022.05.098
123. R.-R. Jeng, S.-L. Lee, C.-W. Hsu, Y.-P. Wu, J.-C. Lin, Effects of the addition of Pd on the hydrogen absorption–desorption characteristics of $Ti_{33}V_{33}Cr_{34}$ alloys. J. Alloys Compd. **464**, 467–471 (2008). https://doi.org/10.1016/j.jallcom.2007.10.010
124. X.B. Yu, Z. Wu, B.J. Xia, N.X. Xu, Improvement of activation performance of the quenched Ti–V-based BCC phase alloys. J. Alloys Compd. **386**, 258–260 (2005). https://doi.org/10.1016/j.jallcom.2004.05.014
125. L. Luo, F. Yang, Y. Li, L. Li, Y. Li, Investigation of the microstructure and hydrogen storage behavior of $V_{48}Fe_{12}Ti_{15+x}Cr_{25-x}$ (x=0, 5, 10, 15) alloys. Int. J. Hydrog. Energy **47**, 9653–9671 (2022). https://doi.org/10.1016/j.ijhydene.2022.01.058
126. P. Pei, X. Song, M. Zhao, P. Zhang, G. Chen, Influences of V content on hydrogen storage properties in low vanadium Ti–V–Cr alloy. Rare Met. Mater. Eng. **37**, 1419–1423 (2008). https://doi.org/10.1016/S1875-5372(09)60039-4
127. S.-W. Cho, C.-S. Han, C.-N. Park, E. Akiba, The hydrogen storage characteristics of Ti–Cr–V alloys. J. Alloys Compd. **288**, 294–298 (1999). https://doi.org/10.1016/S0925-8388(99)00096-1
128. K. Goshome, N. Endo, T. Maeda, Evaluation of the pressure dependence of the cycle durability and thermodynamics of a metal hydride compressor composed of ternary V_{40} and $V_{70}TiCr$. Int. J. Hydrog. Energy **46**, 9479–9487 (2021). https://doi.org/10.1016/j.ijhydene.2020.12.101
129. K. Sakaki, H. Kim, E.H. Majzoub, A. Machida, T. Watanuki et al., Displacement of hydrogen position in di-hydride of V–Ti–Cr solid solution alloys. Acta Mater. **234**, 118055 (2022). https://doi.org/10.1016/j.actamat.2022.118055
130. S.F. Santos, J. Huot, Hydrogen storage in Ti–Mn–(FeV) BCC alloys. J. Alloys Compd. **480**, 5–8 (2009). https://doi.org/10.1016/j.jallcom.2008.09.191
131. F. Ravalison, J. Huot, Hydrogenation thermodynamics of $Ti_{16}V_{60}Cr_{24-x}Fe_x$ alloys (x = 0, 4, 8, 12, 16, 20, 24). Hydrogen **5**, 29–38 (2024). https://doi.org/10.3390/hydrogen5010003
132. J. Matsuda, Y. Nakamura, E. Akiba, Microstructure of Ti–V–Mn BCC alloys before and after hydrogen absorption–desorption. J. Alloys Compd. **509**, 4352–4356 (2011). https://doi.org/10.1016/j.jallcom.2011.01.071
133. Z. Hang, L. Shi, Y. Feng, H. Dong, L. Yang et al., Experimental and theoretical insights into vanadium-based alloys for room temperature hydrogen storage on the example of $Ti_{16}Cr_{22}Zr_5V_{55-x}Fe_2Mn_x$ (x=0–3) alloys. J. Alloys Compd. **988**, 174315 (2024). https://doi.org/10.1016/j.jallcom.2024.174315
134. L. Pickering, J. Li, D. Reed, A.I. Bevan, D. Book, Ti–V–Mn based metal hydrides for hydrogen storage. J. Alloys Compd. **580**, S233–S237 (2013). https://doi.org/10.1016/j.jallcom.2013.03.208
135. X. Li, D. Wu, Q. Zhou, R. Tang, F. Xiao et al., Enhanced cyclic durability of low-cost Ti–V–Cr hydrogen storage alloys by elemental alloying. Mater. Chem. Phys. **317**, 129132 (2024). https://doi.org/10.1016/j.matchemphys.2024.129132
136. J.M. Abdul, S.K. Kolawole, G.A. Salawu, Microstructure and hydrogen storage characteristics of rhodium substituted Ti–V–Cr alloys. JOM **73**, 4112–4118 (2021). https://doi.org/10.1007/s11837-021-04952-z
137. Y. Zhu, X. Li, X.-S. Yang, P. Chen, G.C. Tsui et al., Compositionally complex doping for low-V Ti–Cr–V hydrogen storage alloys. Chem. Eng. J. **477**, 146970 (2023). https://doi.org/10.1016/j.cej.2023.146970
138. A. Kamble, P. Sharma, J. Huot, Effect of doping and particle size on hydrogen absorption properties of BCC solid solution 52Ti–12V–36Cr. Int. J. Hydrog. Energy **42**, 11523–11527 (2017). https://doi.org/10.1016/j.ijhydene.2017.02.137
139. X.B. Yu, Q. Wan, Z. Wu, B.J. Xia, N.X. Xu, Synergism of nano ZnO for improvement of hydrogen absorption performance of Ti–V-based alloys. J. Mater. Res. **19**, 2799–2802 (2004). https://doi.org/10.1557/JMR.2004.0390
140. M. Balcerzak, J. Ternieden, M. Felderhoff, Synthesis, thermal stability, and hydrogen storage properties of poorly crystalline TiVFeCuNb multi-principal element alloy. J. Alloys Compd. **943**, 169142 (2023). https://doi.org/10.1016/j.jallcom.2023.169142
141. X. Wang, W. Guo, Y. Fu, High-entropy alloys: emerging materials for advanced functional applications. J. Mater. Chem. A **9**, 663–701 (2021). https://doi.org/10.1039/d0ta09601f
142. X. Ma, X. Ding, R. Chen, X. Chen, Q. Song et al., Study on microstructure and the hydrogen storage behavior of a TiVZrNbFe high-entropy alloy. Intermetallics **157**, 107885 (2023). https://doi.org/10.1016/j.intermet.2023.107885
143. L. Serrano, M. Moussa, J.-Y. Yao, G. Silva, J.-L. Bobet et al., Development of Ti–V–Nb–Cr–Mn high entropy alloys for

 https://doi.org/10.1007/s40820-025-01672-w

hydrogen storage. J. Alloys Compd. **945**, 169289 (2023). https://doi.org/10.1016/j.jallcom.2023.169289

144. J. Montero, G. Ek, M. Sahlberg, C. Zlotea, Improving the hydrogen cycling properties by Mg addition in Ti–V–Zr–Nb refractory high entropy alloy. Scr. Mater. **194**, 113699 (2021). https://doi.org/10.1016/j.scriptamat.2020.113699
145. L. Huang, M. Long, W. Liu, S. Li, Effects of Cr on microstructure, mechanical properties and hydrogen desorption behaviors of ZrTiNbMoCr high entropy alloys. Mater. Lett. **293**, 129718 (2021). https://doi.org/10.1016/j.matlet.2021.129718
146. C. Zhang, Y. Wu, L. You, W. Qiu, Y. Zhang et al., Nanoscale phase separation of TiZrNbTa high entropy alloy induced by hydrogen absorption. Scr. Mater. **178**, 503–507 (2020). https://doi.org/10.1016/j.scriptamat.2019.12.034
147. C. Zhang, A. Song, Y. Yuan, Y. Wu, P. Zhang et al., Study on the hydrogen storage properties of a TiZrNbTa high entropy alloy. Int. J. Hydrog. Energy **45**, 5367–5374 (2020). https://doi.org/10.1016/j.ijhydene.2019.05.214
148. H. Shen, J. Hu, P. Li, G. Huang, J. Zhang et al., Compositional dependence of hydrogenation performance of Ti–Zr–Hf–Mo–Nb high-entropy alloys for hydrogen/tritium storage. J. Mater. Sci. Technol. **55**, 116–125 (2020). https://doi.org/10.1016/j.jmst.2019.08.060
149. J. Montero, G. Ek, L. Laversenne, V. Nassif, G. Zepon et al., Hydrogen storage properties of the refractory Ti–V–Zr–Nb–Ta multi-principal element alloy. J. Alloys Compd. **835**, 155376 (2020). https://doi.org/10.1016/j.jallcom.2020.155376
150. C. Zhang, Y. Wu, L. You, X. Cao, Z. Lu et al., Investigation on the activation mechanism of hydrogen absorption in TiZrNbTa high entropy alloy. J. Alloys Compd. **781**, 613–620 (2019). https://doi.org/10.1016/j.jallcom.2018.12.120
151. M.M. Nygård, G. Ek, D. Karlsson, M.H. Sørby, M. Sahlberg et al., Counting electrons—a new approach to tailor the hydrogen sorption properties of high-entropy alloys. Acta Mater. **175**, 121–129 (2019). https://doi.org/10.1016/j.actamat.2019.06.002
152. H.-Z. Hu, H.-Q. Xiao, X.-C. He, W.-H. Zhou, X.-X. Zhang et al., Development of Ti–V–Cr–Mn–Mo–Ce high-entropy alloys for high-density hydrogen storage in water bath environments. Rare Met. **43**, 5229–5241 (2024). https://doi.org/10.1007/s12598-024-02618-8
153. M. Vaidya, K. Guruvidyathri, B.S. Murty, Phase formation and thermal stability of CoCrFeNi and CoCrFeMnNi equiatomic high entropy alloys. J. Alloys Compd. **774**, 856–864 (2019). https://doi.org/10.1016/j.jallcom.2018.09.342
154. M. Vaidya, G. Mohan Muralikrishna, S.V. Divinski, B.S. Murty, Experimental assessment of the thermodynamic factor for diffusion in CoCrFeNi and CoCrFeMnNi high entropy alloys. Scr. Mater. **157**, 81–85 (2018). https://doi.org/10.1016/j.scriptamat.2018.07.040
155. K. Guruvidyathri, B.S. Murty, J.W. Yeh, K.C. Hari Kumar, Gibbs energy-composition plots as a tool for high-entropy alloy design. J. Alloys Compd. **768**, 358–367 (2018). https://doi.org/10.1016/j.jallcom.2018.07.264
156. C. Chattopadhyay, A. Prasad, B.S. Murty, Phase prediction in high entropy alloys—a kinetic approach. Acta Mater. **153**, 214–225 (2018). https://doi.org/10.1016/j.actamat.2018.05.002
157. K.S. Senkevich, M.M. Serov, O.Z. Umarova, Fabrication of intermetallic titanium alloy based on Ti_2AlNb by rapid quenching of melt. Met. Sci. Heat Treat.. Sci. Heat Treat. **59**, 463–466 (2017). https://doi.org/10.1007/s11041-017-0172-3
158. H.Y. Zhou, F. Wang, J. Wang, Z.M. Wang, Q.R. Yao et al., Hydrogen storage properties and thermal stability of $V_{35}Ti_{20}Cr_{45}$ alloy by heat treatment. Int. J. Hydrog. Energy **39**, 14887–14895 (2014). https://doi.org/10.1016/j.ijhydene.2014.07.054
159. R.-R. Jeng, C.-Y. Chou, S.-L. Lee, Y.-C. Wu, H.-Y. Bor, Effect of Mn, Ti/Cr ratio, and heat treatment on hydrogen storage properties of TI–V–CR–MN alloys. J. Chin. Inst. Eng. **34**, 601–608 (2011). https://doi.org/10.1080/02533839.2011.577595
160. S.-W. Cho, C.-S. Han, C.-N. Park, E. Akiba, Hydrogen storage characteristics of Ti–Zr–Cr–V alloys. J. Alloys Compd. **289**, 244–250 (1999). https://doi.org/10.1016/S0925-8388(99)00162-0
161. M. Okada, T. Kuriiwa, T. Tamura, H. Takamura, A. Kamegawa, Ti–V–Cr b.c.c. alloys with high protium content. J. Alloys Compd. **330**, 511–516 (2002). https://doi.org/10.1016/S0925-8388(01)01647-4
162. L. Luo, X. Bian, W.-Y. Wu, Z.-M. Yuan, Y.-Z. Li et al., Influence of annealing on microstructure and hydrogen storage properties of $V_{48}Fe_{12}Ti_{15}Cr_{25}$ alloy. J. Iron. Steel Res. Int. **27**, 217–227 (2020). https://doi.org/10.1007/s42243-019-00337-4
163. V.A. Dekhtyarenko, T.V. Pryadko, D.G. Savvakin, V.I. Bondarchuk, G.S. Mogylnyy, Hydrogenation process in multiphase alloys of Ti–Zr–Mn–V system on the example of $Ti_{42.75}Zr_{27}Mn_{20.25}V_{10}$ alloy. Int. J. Hydrog. Energy **46**, 8040–8047 (2021). https://doi.org/10.1016/j.ijhydene.2020.11.283
164. Y. Munekata, K. Washio, T. Suda, N. Hashimoto, S. Ohnuki et al., Role of annealing for improving hydrogen storage properties of Ti–Cr–V alloy. MRS Online Proc. Libr. **971**, 721 (2011). https://doi.org/10.1557/PROC-0971-Z07-21
165. B. Liu, X. Chen, S. Zhang, X. Ding, R. Chen, Formation of eutectic and hydrogen absorption/desorption behavior of heat-treated $Ti_{19}Hf_4V_{40}Mn_{35}Cr_2$ alloys. Intermetallics **152**, 107752 (2023). https://doi.org/10.1016/j.intermet.2022.107752
166. C. Yang, Q. Wang, M. Wang, Y. Wang, R. Du et al., Effect of V content on hydrogen storage properties and cyclic durability of V–Ti–Cr–Fe alloys. Int. J. Hydrog. Energy **48**, 26870–26880 (2023). https://doi.org/10.1016/j.ijhydene.2023.03.307
167. L. Luo, C. Wu, S. Yang, J. Zhou, Y. Chen et al., Decaying behaviors of $V_{40}(TiCr)_{51}Fe_8Mn$ hydrogen storage alloys with different particle sizes. J. Alloys Compd. **645**, S178–S183 (2015). https://doi.org/10.1016/j.jallcom.2014.12.261
168. H. Kwon, J.-H. Yoo, K.-M. Roh, C.-Y. Suh, W.-B. Kim et al., Effect of particle size and microstructure on the

hydrogen storage property in a V–Ti–Cr solid solution system. J. Alloys Compd. **535**, 87–90 (2012). https://doi.org/10.1016/j.jallcom.2012.04.078

169. H. Kim, K. Sakaki, H. Ogawa, Y. Nakamura, J. Nakamura et al., Origin of degradation in the reversible hydrogen storage capacity of $V_{1-x}Ti_x$ alloys from the atomic pair distribution function analysis. J. Phys. Chem. C **117**, 26543–26550 (2013). https://doi.org/10.1021/jp408766r
170. C. Wu, Q. Wang, Y. Mao, L. Huang, Y. Chen et al., Relationship between lattice defects and phase transformation in hydrogenation/dehydrogenation process of the $V_{60}Ti_{25}Cr_3Fe_{12}$ alloy. Int. J. Hydrog. Energy **44**, 9368–9377 (2019). https://doi.org/10.1016/j.ijhydene.2019.02.097
171. K. Ikeda, S. Sashida, T. Otomo, H. Ohshita, T. Honda et al., Local structural changes in V–Ti–Cr alloy hydrides with hydrogen absorption/desorption cycling. Int. J. Hydrog. Energy **51**, 79–87 (2024). https://doi.org/10.1016/j.ijhydene.2023.10.318
172. U. Ulmer, D. Oertel, T. Diemant, C. Bonatto Minella, T. Bergfeldt et al., Performance improvement of V–Fe–Cr–Ti solid state hydrogen storage materials in impure hydrogen gas. ACS Appl. Mater. Interfaces **10**, 1662–1671 (2018). https://doi.org/10.1021/acsami.7b13541
173. Q. Xie, M. Jiang, H. Kong, Q. Huang, C. Wu et al., Enhanced air-poisoning resistance in vanadium-based hydrogen storage alloy by addition of Si. Prog. Nat. Sci. Mater. Int. **34**, 648–653 (2024). https://doi.org/10.1016/j.pnsc.2024.05.010
174. S. Suwarno, J.K. Solberg, B. Krogh, S. Raaen, V.A. Yartys, High temperature hydrogenation of Ti–V alloys: the effect of cycling and carbon monoxide on the bulk and surface properties. Int. J. Hydrog. Energy **41**, 1699–1710 (2016). https://doi.org/10.1016/j.ijhydene.2015.11.077
175. H.C. Lin, K.M. Lin, K.C. Wu, H.H. Hsiung, H.K. Tsai, Cyclic hydrogen absorption–desorption characteristics of TiCrV and $Ti_{0.8}Cr_{1.2}V$ alloys. Int. J. Hydrog. Energy **32**, 4966–4972 (2007). https://doi.org/10.1016/j.ijhydene.2007.07.057
176. Z. Wu, C. Yang, Y. Yan, Y. Wang, X. Tang et al., Effect of dehydrogenation depth on cyclic hydrogen desorption properties of $V_{40}Ti_{2.55}Cr_{2.65}Fe_8$ alloy. J. Alloys Compd. **955**, 170036 (2023). https://doi.org/10.1016/j.jallcom.2023.170036
177. M. Tsukahara, K. Takahashi, A. Isomura, T. Sakai, Influence of oxygen on hydrogen storage and electrode properties for micro-designed V-based battery alloys. J. Alloys Compd. **265**, 257–263 (1998). https://doi.org/10.1016/S0925-8388(97)00286-7
178. T. Huang, Z. Wu, B. Xia, J. Chen, X. Yu et al., $TiCr_{1.2}(V–Fe)_{0.6}$: a novel hydrogen storage alloy with high capacity. Sci. Technol. Adv. Mater. **4**, 491–494 (2003). https://doi.org/10.1016/j.stam.2003.12.001
179. U. Ulmer, K. Asano, A. Patyk, H. Enoki, Y. Nakamura et al., Cost reduction possibilities of vanadium-based solid solutions—microstructural, thermodynamic, cyclic and environmental effects of ferrovanadium substitution. J. Alloys Compd. **648**, 1024–1030 (2015). https://doi.org/10.1016/j.jallcom.2015.07.110
180. Y. Nakamura, J. Nakamura, K. Sakaki, K. Asano, E. Akiba, Hydrogenation properties of Ti–V–Mn alloys with a BCC structure containing high and low oxygen concentrations. J. Alloys Compd. **509**, 1841–1847 (2011). https://doi.org/10.1016/j.jallcom.2010.10.059
181. T. Dou, Z. Wu, J. Mao, N. Xu, Application of commercial ferrovanadium to reduce cost of Ti–V-based BCC phase hydrogen storage alloys. Mater. Sci. Eng. A **476**, 34–38 (2008). https://doi.org/10.1016/j.msea.2007.04.080
182. T. Bibienne, C. Gosselin, J.-L. Bobet, J. Huot, Replacement of vanadium by ferrovanadium in a Ti-based body centred cubic (BCC) alloy: towards a low-cost hydrogen storage material. Appl. Sci. **8**, 1151 (2018). https://doi.org/10.3390/app8071151
183. J. Mi, X. Liu, Z. Li, L. Jiang, Z. Huang et al., Effects of Si and Ce on the microstructure and hydrogen storage property of $Ti_{26.5}Cr_{20}V_{45}Fe_{85}Ce_{0.5}$ alloy. Sci. China Ser. E Technol. Sci. **52**, 256–259 (2009). https://doi.org/10.1007/s11431-009-0026-3
184. A. Bishnoi, P. Sharma, Effect of industrial grade raw materials and its associated impurities on first hydrogenation of BCC solid solution alloys. Int. J. Hydrog. Energy **56**, 471–483 (2024). https://doi.org/10.1016/j.ijhydene.2023.12.134

 https://doi.org/10.1007/s40820-025-01672-w